공학박사학위논문

염료감응 태양전지의 전극 내 효율적 광 이용에 관한 연구

Photon Managements in Dye-Sensitized Solar Cells by Modified Electrodes

2013년 2월

서울대학교 대학원
공과대학 화학생물공학부
우 상 혁

Abstract

Photon Managements in Dye-Sensitized Solar Cells by Modified Electrodes

Sanghyuk Wooh
School of Chemical and Biological Engineering
The Graduate School
Seoul National University

Renewable energy resources have recently gained a great deal of attention due to the ever increasing energy demand, the shortage of fossil fuels, and the growing interest in enviromentally friendly energy scources. Among various kinds of renewable energy sources, solar cells have been regarded as a good candidate because they could capitalize on sunlight as the unlimited energy source. In this context, photon management in photovoltaic devices has recently attracted immense attention because of the intrinsic limitation in film thickness of the photo-induced charge generation layer. To compensate for the limited light absorption within a given thickness related to the charge carrier recombination, particularly in thin film solar cells, there have been many trials on how to efficiently use photons. In this study, we demonstrated strategies for efficient photon management in dye sensitized solar cells (DSCs) which have recently received much attention due to several advantages, low-cost of fabrication and high power conversion efficiency.

In first chapter, the TiO_2 surface passivation with superhydrophobic surface on DSCs was demonstrated. Dye sensitizers were adsorbed on the TiO_2 structures by dip-coating, fabricating photoanodes. After dye adsorption, uncovered TiO_2 surfaces were filled with 1H,1H,2H,2H-perfluorooctyltriethoxysilane by sequential adsorption process, as coadsorbents. With this novel method, fluorinate surfaces which have low surface energy were developed with compact monolayer and played an essential role in blocking layer of back electron reaction in the interface between TiO_2 and electrolyte, called electron recombination. We have analyzed the effects of the fluorinate surface for photovoltaic performance of DSCs by photovoltaic and electrochemical characterization. The charge transfer resistance was remarkably increased by effective TiO_2 surface passivation, resulting in inhibition of the electron recombination and enhanced photocurrent as well as photovoltage. Furthermore, in case of adsorbing organic dyes, coadsorbents prevented aggregation of dyes efficiently and induced considerable enhancement of electron injection into the TiO_2 photoanodes. Last, we suggested a new concept, a secondary coadsorbent by sequential adsorption, with chenodeoxycholic acid which is a conventional coadsorbent, leading to highly increased power conversion efficiency of DSCs.

In second chapter, we have demonstrated the method to incorporate the gold/silica core-shell nanoparticles ($Au@SiO_2$ NPs) into TiO_2 photoanodes and their effect on photovoltaic performance of DSCs with PEGDME electrolyte. First, various sizes of gold core with thin silica shell around 10 nm thickness as electronic and chemical insulator were synthesized. $Au@SiO_2$ incorporated

photoanodes were realized with as-synthesized Au@SiO_2 NPs mixed with TiO_2 paste. Polymer electrolytes based on poly(ethylene glycol dimethyl ether) (PEGDME) have been introduced instead of liquid electrolytes to get higher stability from the corrosive I^- / I_3^- ions. In addition, we demonstrate a method of incorporation of Au@SiO_2 NPs into the TiO_2 photoanodes and characterize the enhancement of photovoltaic performances by the localized surface plasmon resonance (LSPR) of gold nanoparticles (Au NPs). In addition, the SiO_2 hollow spheres were fabricated by corrosion treatment with I^- / I_3^- solution to eliminate Au core and make condition for accurate comparison between with and without Au NPs. Using this novel method, we have analyzed the effects of the Au@SiO_2 NPs on optical, electrochemical, and photovoltaic properties of the photoanodes. The influence by SiO_2 shell and morphology change were characterized separate from the influence by LSPR of Au core. From this, we demonstrated dominant side effect of incorporation of Au@SiO_2 NPs in DSCs, the hindering light effect by absorption of Au core. Lastly, it has been demonstrated with EIS measurement that the incorporation of Au@SiO_2 NPs affect the enhancement of light harvesting of dye molecules exclusively and following increases Jsc of DSCs without changing the electron lifetime and diffusion coefficient of TiO_2 photoanodes.

Finally in last chapter, we introduce a novel strategy to trap incident light effectively by three dimensional patterned TiO_2 photoanodes in DSCs. Among different geometries of electrodes fabricated by the soft lithographic technique, pyramid-shaped TiO_2 photoanodes show the highest absorbance and

photocurrent-voltage performance, which originate from the light path elongation inside the 3D photoanodes and the total reflection at the interfaces between TiO_2 photoanodes and bulk electrolyte. In order to create even cheaper three dimensional pattern masters, randomized pyramid structures were developed using the texturing of crystalline silicon substrates with anisotropic wet etching. Furthermore, by the combination of the effect of light path elongation of randomized pyramids with a scattering layer, we demonstrate the 40% and 36% increase in the photocurrent and the power conversion efficiency of DSCs over the conventional planar photoanodes, respectively.

Keyword: photon management, dye-sensitized solar cell, superhydrophobic coadsorbent, localized surface plasmon resonance, three dimentional photoanode

Student Number: 2008-30262

Contents

List of Tables

List of Figures

Chapter 1. Superhydrophobic Surface for Effective Passivation of TiO_2 Nanocrystals in Dye-Sensitized Solar Cells

1.1 Introduction

Dye-sensitized solar cells (DSCs) have recently received a numerous attention because of the promising power conversion efficiency with low-cost of fabrication, since the first breakthrough work by O'Regan and Grätzel[1,2]. The common architecture of the most widely studied DSC is a sandwich structure between two transparent conducting glasses. One of these consists of nanoporous semiconductor e.g. TiO_2 film with sensitizers (photoanode) whereas platinum coated glass slide acts as a counter electrode. On exposing to light, the dye sensitizers generate and inject electrons which pass through the TiO_2 nanostructure of several microns thickness, and this process undoubtedly plays a major role in DSCs.[3-5] On this account, electrochemical reactions on the TiO_2 / dye / electrolyte interface strongly affect on the photovoltaic performance of DSCs, such as the open circuit voltage and the short circuit current[6-8]. Among these reactions, the back electron transfer from the surface state of TiO_2 to the electrolyte, called recombination, inflict a heavy loss for power conversion efficiency[9-12]. Therefore, for a decade, TiO_2 surface passivation with many different kinds of materials, called coadsorbents, has been extensively explored to modify the interfacial properties and reduce recombination efficiently, causing

higher power conversion efficiency[13-16]. Although numerous kind of materials for coadsorbent have been introduced, such as the 3-phenylpropionic acid (PPA), decylphosphonic acid (DPA), chenodeoxycholic acid (CDCA), and dineohexyl bis(3,3-dimethylbutyl) phosphinic acid (DINHOP), the insulation of the TiO_2 surface from the electrolyte has not been complete to block recombination sufficiently[17-22].

In this study, we demonstrate the fluorinated surface on TiO_2 surface. Fluorinated surface derives their unique characteristics from the molecular properties associated with the C-F bond. A low friction coefficient and a low surface energy of fluorinate surface are useful for antifouling and antifogging applications[23-27]. In previous research, the surface tension of molecules are established in the order of CH_3 (30 mN/m) > CF_2 (23 mN/m) > CF_3 (15 mN/m). A uniform array of CF_3 groups can make a surface tension below 6 mN/m[28].

Due to these unique properties, we fabricated fluorinated surface on the recombination site of the TiO_2 surface with 1H,1H,2H,2H-perfluorooctyl triethoxysilane (F-SAM) by sequential adsorption process, as coadsorbents. With this approach, fluorinate surfaces played an essential role in blocking layer of back electron reaction in the interface between TiO_2 and electrolyte. First, we have analyzed the effects of the fluorinate surface with commercial ruthenium based sensitizing dye ((*cis*-di(thiocyanate)bis(2,2_-bipyridyl-4,4_-dicarboxylate)-ruthenium(II) bis-tetrabutyl-ammonium), named N719) for photovoltaic performance of DSCs by photovoltaic and electrochemical characterization. The charge transfer resistance was remarkably increased by effective TiO_2 surface

passivation, resulting in inhibition of the electron recombination and enhanced photocurrent as well as photovoltage. Furthermore, in case of adsorbing organic dyes (2-Cyano-3-[5‴-(9-ethyl-9*H*-carbazol-3-yl)-3′,3″,3‴,4-tetra-*n*-hexyl-[2,2′,5′,2″,5″,2‴]-quater thiophen-5-yl] acrylic acid, named MK-2) which have been found to be more susceptible to aggregate formation compared to ruthenium based dye, coadsorbents prevented aggregation of dyes and induced considerable enhancement of electron injection into the TiO_2 photoanodes.[29, 30] Last, we suggested a novel concept, a secondary coadsorbent by sequential adsorption, with chenodeoxycholic acid which is a conventional coadsorbent, leading to additional increased power conversion efficiency of DSCs.

1.2 Experimental Section

1.2.1 Materials

All chemicals were used without any further purification and water was always doubly ionized. Chemicals used for the fabrication of the dye-sensitized solar cells, 1H,1H,2H,2H-perfluorooctyl triethoxysilane, 1-methyl-3-propyl imidazolium iodide (MPII), iodine (I_2) and organic dye as a sensitizer, 2-Cyano-

3-[5‴-(9-ethyl-9*H*-carbazol-3-yl)-3′,3″,3‴,4-tetra-*n*-hexyl-[2,2′,5′,2″,5″,2‴]-quater thiophen-5-yl] acrylic acid, so called MK-2 were obtained from Sigma-Aldrich. TiO_2 paste (DSL 18NR-T) and dye as a sensitizer, *cis*-diithiocyanato-bis(2,2'-bipyridyl-4,4'-dicarboxylato)-ruthenium(II) bis(tetrabutylammonium), so called N719 were purchased from Dyesol.

1.2.2 Fabrication and Surface Passivation of Photoanode

0.1 M of Ti (IV) bis(ethyl acetoacetato)-diisopropoxide in 1-butanol solution was spin-coated onto the FTO glass followed by sintering at 500 ºC for the formation of electron blocking layer between TCO substrate and oxidized species in the electrolyte. TiO_2 photoandes were fabricated by TiO_2 pastes using doctor blade method onto the FTO substrate (TEC 8, Pilkington) and then sintered at 500 °C for 15 min. Subsequently, TiO_2 nanostructures coated FTO substrates were dipped into 40 mM $TiCl_4$ in H_2O solution at 70 °C for 30 min and sintered at 500 °C for 15 min.

TiO_2 photoanodes were dipped into the 0.3 mM N719 dye (cis-bis(isothiocyanato)bis(2,2'-bipyridyl-4,4'-dicarboxylato)-ruthenium (II) bis-tetrabutylammonium, Dyesol) in the acetonitrile and tert-butanol solution (1:1 v/v) at 30 °C for 18 hours and then rinsed with acetonitrile and dried using stream of nitrogen. In case of organic dyes, TiO_2 photoanodes were dipped into the 0.2 mM MK-2 dye (2-Cyano-3-[5‴-(9-ethyl-9*H*-carbazol-3-yl)-3′,3″,3‴,4-tetra-*n*-hexyl-[2,2′,5′,2″,5″,2‴]-quater thiophen-5-yl] acrylic acid) in the toluene, acetonitrile and tert-butanol solution (1:1:1 v/v/v) at 30 °C for 6 hours and then

rinsed with toluene and dried in the vacuum condition.

For surface passivation, as-prepared TiO_2 photoanodes were sequentially dipped into the 0.05 M of 1H,1H,2H,2H-perfluorooctyltriethoxysilane in hexane solution 30 °C for 6 hours and then rinsed with hexane.

1.2.3 Device fabrication

Pt counter electrodes were prepared by thermal decomposition of 0.01 M H_2PtCl_6 in isopropyl alcohol solution spun cast on the FTO substrate at 500 °C for 15 min, and then two holes were made by drill for electrolyte injection. The TiO_2 photoanodes were attached with the counter electrodes using surlyn films (25 μm, Solaronix) which had a role of a spacer between both electrodes. The electrolyte was a mixing solution of 0.6 M 1-methyl-3-propylimidazolium iodide, 0.05 M I_2 in acetonitrile. This mixed electrolyte was filled into the holes of the Pt counter electrodes of sandwich structured cells by capillary force, and the holes were subsequently sealed by sulyn films and cover glasses

1.2.4 Solar Cell Characterization

The optical properties of electrodes such as transmission and reflection were characterized by UV/Vis spectroscopy with the integrating sphere (V-670 UV/Vis spectrophotometer, Jasco). Thicknesses of photoanodes were characterized with surface profiler (alpha-step IQ, Tencor). Current-voltage characterization of the DSCs was carried by a Keithley 2400 digital source meter and solar simulator equipped with 300 W Xenon arc-lamp (Newport) under 1 sun

illumination (AM 1.5, 100 mW cm^{-2}). The light intensity was calibrated by silicon solar cell (PV measurement). In addition, quantum efficiency of DSCs was analyzed by incident photon to current efficiency (IPCE) (PV measurements, Inc.) as a function of wavelength. Charge transfer resistance and electron lifetime in photoanodes were characterized by electrochemical impedance spectroscopy (EIS) using IM6 (Zahner) under dark and illumination condition with bias potential of -0.54 V. The frequency was in the range of 1 M - 0.1 Hz and amplitude was fixed to 10 mV. The obtained spectra were fitted and analyzed using Z-View software with equivalent circuits.

The electron diffusion coefficient and electron lifetime in photoanodes were evaluated by intensity-modulated photocurrent spectroscopy (IMPS) under short-circuit conditions and intensity-modulated photovoltage spectroscopy (IMVS) under open-circuit conditions as a function of light intensity using a CIMPS (Controlled Intensity Modulated Photo Spectroscopy) system (Zahner) and white light source (Zahner).

1.3 Results and Discussion

1.3.1 Formation of Fluorinated Surface on the TiO_2 Photoanodes

The fluorinated surface was formed by sequential dipping method to passivate bare TiO_2 surface, as shown in Scheme 1.1. As-sintered TiO_2 photoanodes were dipped in dye solution for 18 hr first, and then dipped in 1H,1H,2H,2H-perfluorooctyltriethoxysilane solution dissolved in hexane sequentially (so called F-SAM treatment). 1H,1H,2H,2H-perfluorooctyl triethoxysilane, act as coadsorbent, makes homogeneous fluorinate surface on the bare surface of TiO_2 without dyes.

In this study, two different dyes were used which were ruthenium based commercial N719 dye and organic MK-2 dye, having carboxylic anchoring groups (Figure 1.1 a, b). To verify passivation effect of F-SAM, photoanodes were characterized with N719 dye first. Conventional coadsorbents have been adsorbed on TiO_2 surface competitively with dyes, in dye / coadsorbent mixture solution. However, due to sequential adsorption and low solubility of N719 dye for hexane, N719 dyes can attach on the surface of TiO_2 during the dipping process in F-SAM solution, resulting in no loss of dyes on photoanodes. Absorbance of photoanodes, characterized by photos and UV/Vis. Spectroscopy, are not changed between before and after F-SAM treatment, meaning same amount of adsorbed dyes are adsorbed (Figure 1.2). From this unique property of sequential adsorption in case of N719, we can fabricate passivated TiO_2 surface

without dye desorption, and analyze exact effect of F-SAM coadsorbents on the photovoltaic performance of DSCs.

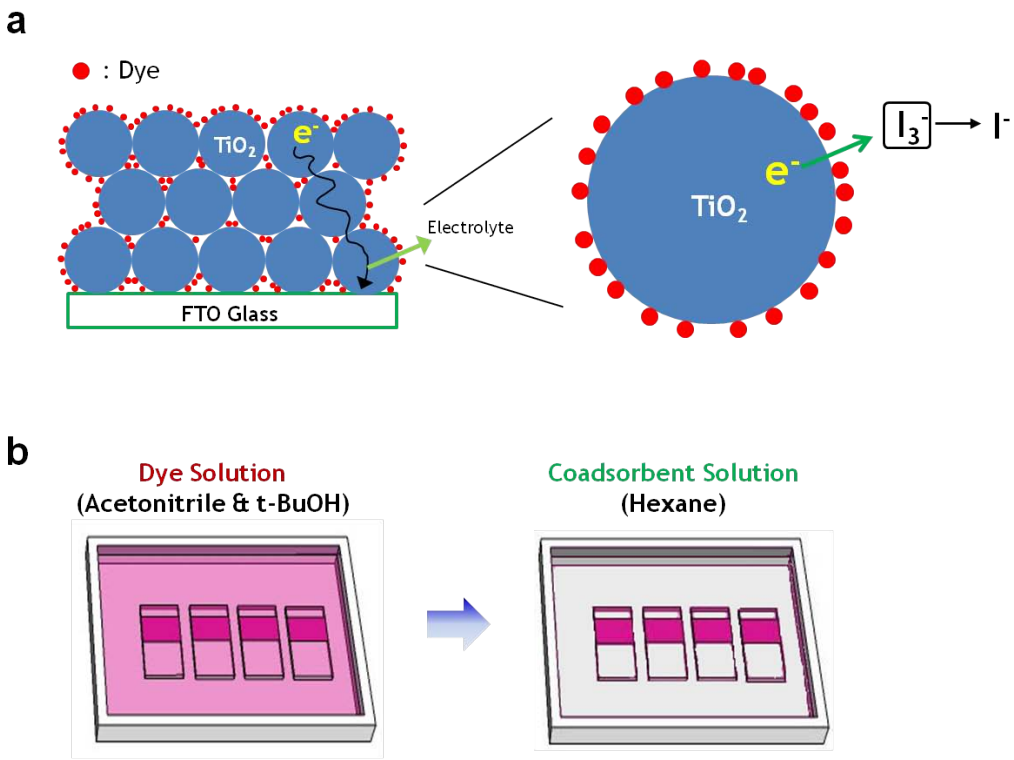

Scheme 1.1. Schematic illustration of electron back electron transfer from TiO_2 to electrolyte, a and sequential process for TiO_2 passivation with F-SAM coadsorbent.

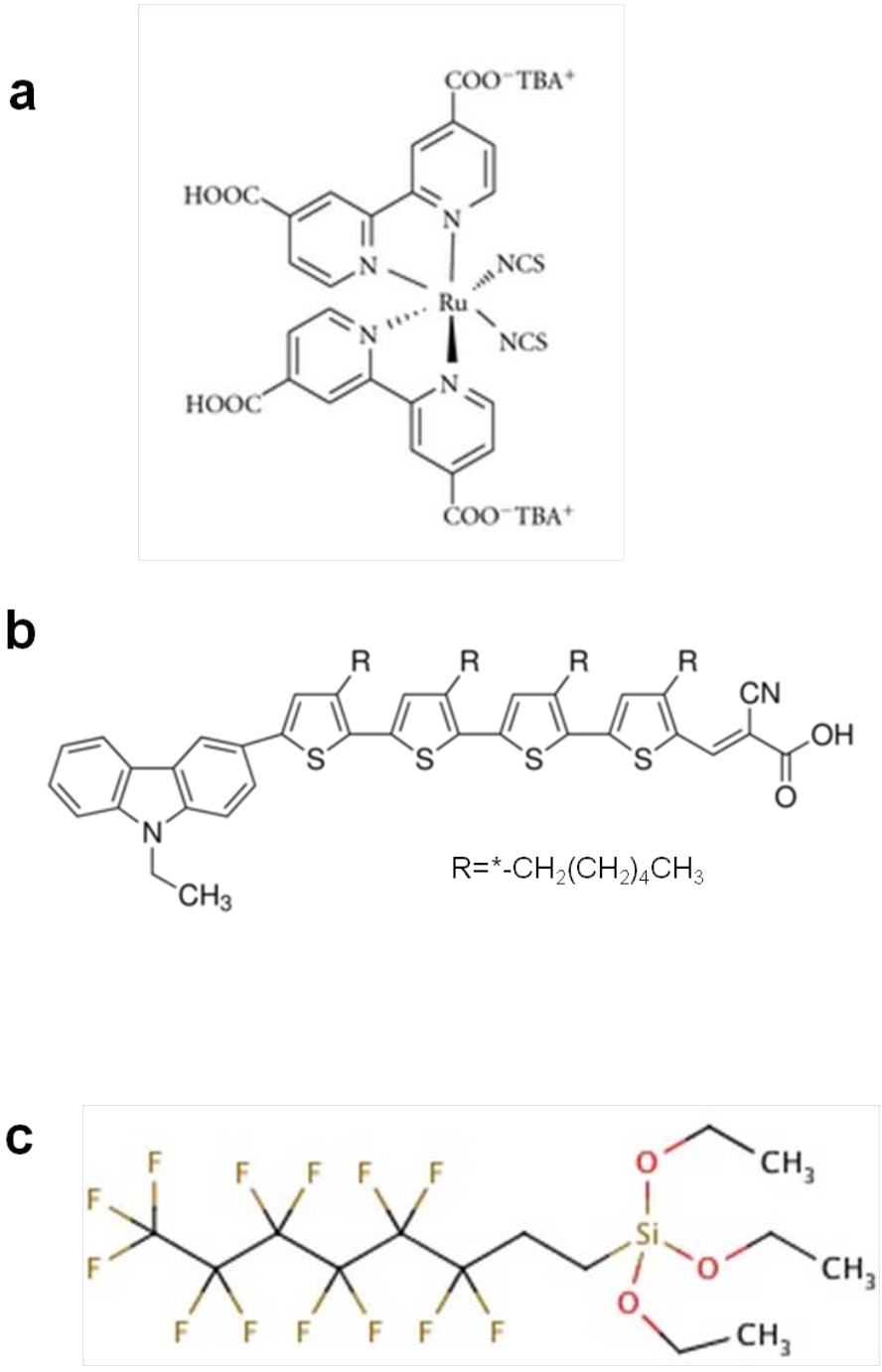

Figure 1.1. The chemical structures of a) N719, b) MK-2, and c) a coadsorbent forming fluorinated surface.

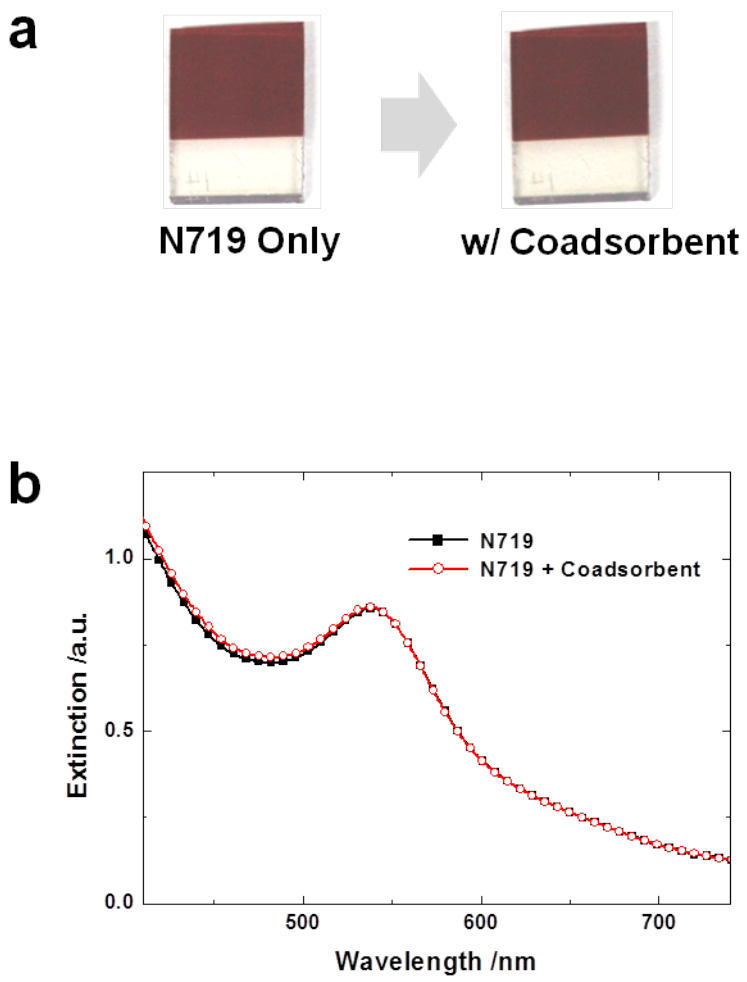

Figure 1.2. a) photos and b) UV-Vis. spectrum of photoanodes, comparing before and after adsorbing F-SAM coadsorbents on the TiO_2 / N719 surface.

1.3.2 Effect of Fluorinated Surface with Ruthenium Based N719 Dye on the Photovoltaic Performance of DSCs

The fluorinated surface, adsorbing 1H,1H,2H,2H-perfluorooctyltriethoxysilane molecule on the bare TiO_2 surface after N719 dye adsorption was verified with ATR-FTIR spectroscopy, as shown in Figure 1.3. The Si-O-Si and Si-O-Ti formation is observed at about 1070 cm^{-1}, 1146 cm^{-1}, and 1244 cm^{-1}. From this, we can find the formation of fluorinated surface on the TiO_2.

The photocurrent-voltage characteristics of DSCs with F-SAM formed photoanodes were measured under 1 Sun illumination (AM 1.5 and 100 mW cm^{-2}) with shading masks (active area: 0.25 cm^2) (Figure 1.4 a, b). The F-SAM passivated photoanode shows around 70 mA cm^{-2} and 40 mV higher photocurrent and open-circuit voltage, respectively, than values measured from photoanode adsorbing only N719 dye (Table 1.1). The power conversion efficiency was also increased up to 15 % (4.81 % → 5.58 %) followed by enhanced photocurrent and open-circuit voltage. In case of F-SAM treated photoanode, the enhancement of open-circuit voltage is influenced with efficient blocking of electron back transfer from the TiO_2 to the electrolyte, so called recombination. In a few micro-second, recombination is occurred at a bare TiO_2 surface of photoanodes by the reaction with I_3^- ions in the electrolyte when the TiO_2 surface is only covered with N719 dyes. However, the low surface energy of fluorinated monolayer can easily repel the electrolyte containing I_3^- ions, resulting in efficient reduction of

recombination and increase of open-circuit voltage. The photocurrent enhancement is also affected by decreased recombination, due to increased charge collection efficiency. Consequently, the external quantum efficiencies were demonstrated at a whole range of wavelength, characterized by the incident photon-to-current measurement (Figure 1.4 c).

For further investigation, electrochemical impedance spectroscopy (EIS) measurement was performed in the dark with - 0.68 V of bias potential (Figure 1.5). Each result was fitted with general transmission model of DSCs. In Figure 1.5 a, the Nyquist plots show two predominant semicircles. The first semicircle at high frequency is attributed to the charge transfer resistance at the interface between Pt counter electrode and electrolyte (R_{pt}) and the second one at mid-frequencies is associated with the electron transport (R_t) and the electron recombination (R_{rec}) at the interface between TiO_2 and electrolyte. The recombination resistances (R_{rec}) of TiO_2 photoanodes employing fluorinated monolayer are remarkably increased, comparing the value from photoanodes with only N719 dyes, both in the dark condition.

For Bode plots in the dark (Figure 1.5 b), the characteristic frequency peak in the mid-frequencies (1 k - 10 Hz) of F-SAM formed photoanode is shifted to lower frequency, indicating the longer electron lifetime. In addition, the role of the fluorinated monolayer in the electron lifetime and the electron diffusion coefficient in TiO_2 photoanodes are also evaluated from incident-modulated photovoltage spectroscopy (IMVS) and incident-modulated photocurrent spectroscopy (IMPS) as a function of light intensity as given in

Figure 1.6. In accordance with the results from EIS measurements (Bode plot, Figure 1.5 b), the electron lifetime upon the F-SAM treated photoanode is increased, compared to that of photoanode with only N719 dyes. It presents that the fluorinated monolayer change the electron lifetime in photoanodes of DSCs, effectively.

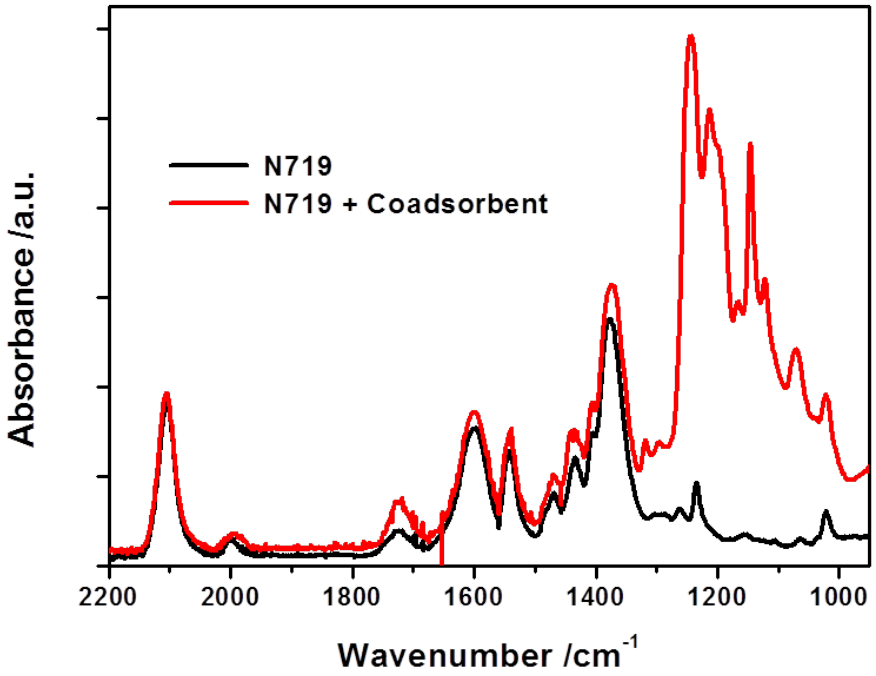

Figure 1.3. ATR-FTIR spectra of the TiO_2 films sensitized with N719. Black and red solid lines are before and after treatment with F-SAM coadsorbent, respectively.

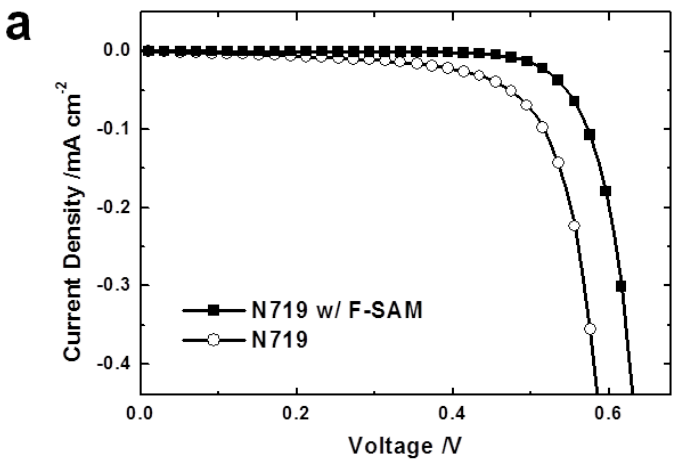
a
Current Density /mA cm-2
0.0
-0.1
-0.2
-0.3
-0.4
0.0
0.2
0.4
0.6
Voltage /V
N719 w/ F-SAM
N719

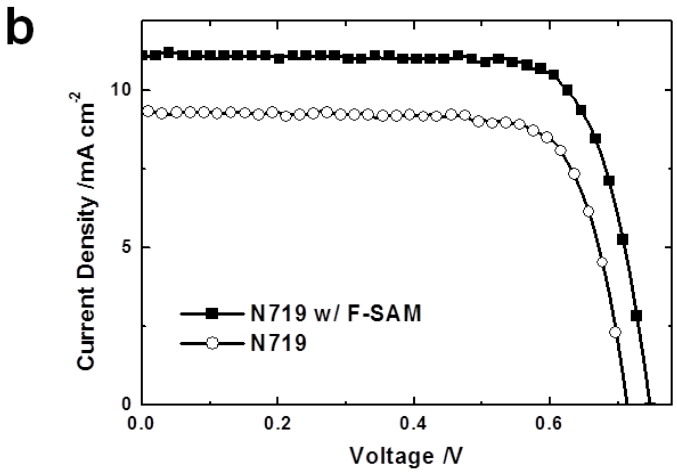
b
Current Density /mA cm-2
10
5
0
0.0
0.2
0.4
0.6
Voltage /V
N719 w/ F-SAM
N719

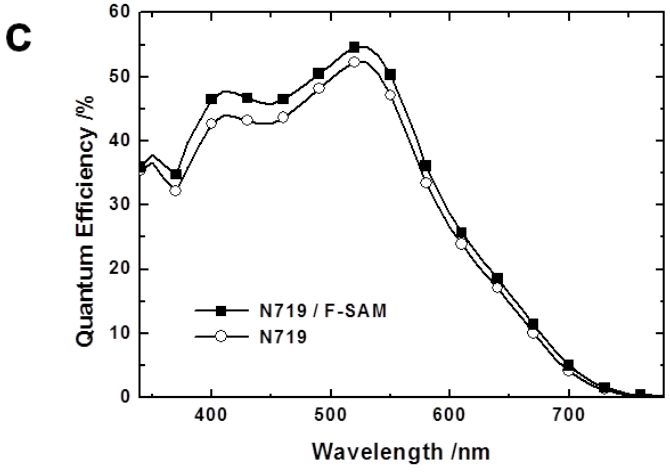
c
Quantum Efficiency /%
60
50
40
30
20
10
0
400
500
600
700
Wavelength /nm
N719 / F-SAM
N719

Figure 1.4. Photocurrent-voltage characteristics of DSCs sensitized with N719 and N719 / F-SAM coadsorbent, a) at dark condition and b) under illumination. c) external quantum efficiency characterized by incident photon-to-current efficiency measurement.

Table 1.1. I-V characteristics of the DSCs with TiO_2 photoelectrodes employing F-SAM coadsorbent.

Type of TiO_2 photoanode	V_{OC} (mV)	J_{SC} (mA cm^{-2})	FF (%)	Efficiency (%)
N719	0.712	9.10	74.2	4.81
N719 / F-SAM	0.752	9.83	75.5	5.58

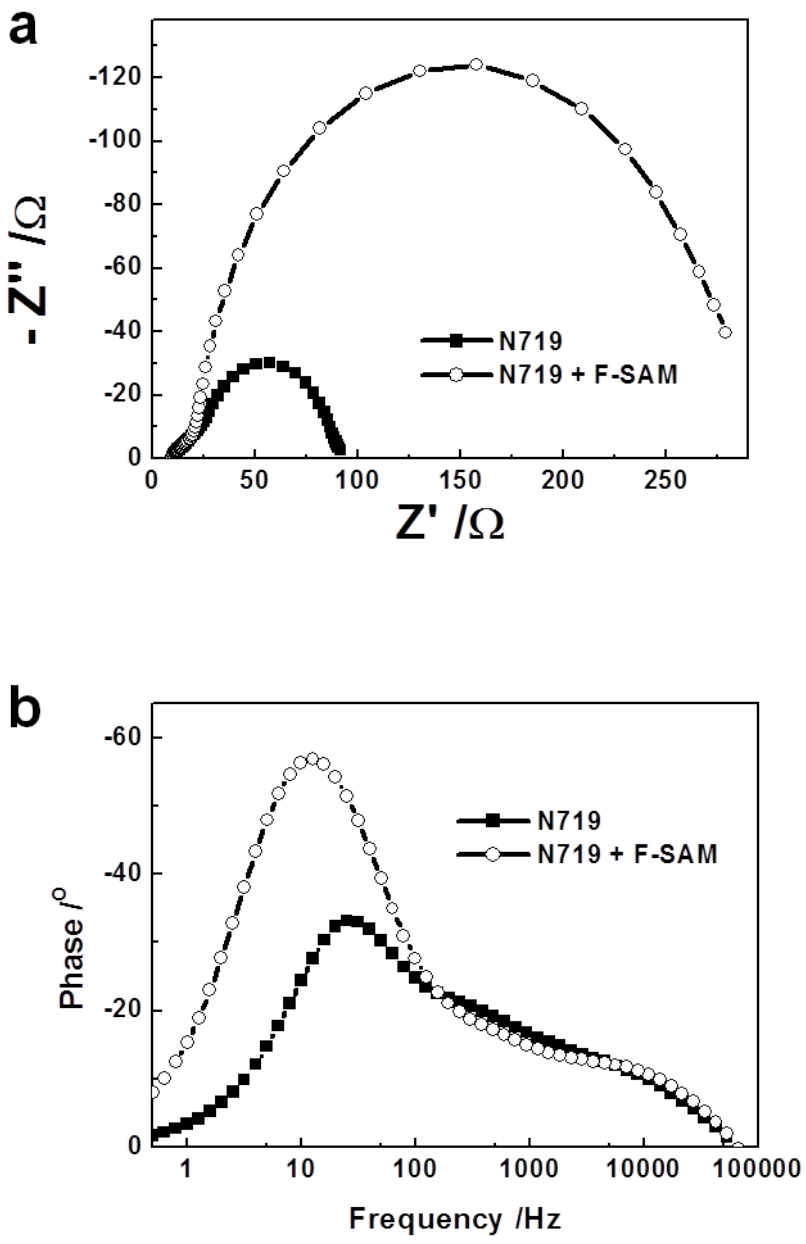

Figure 1.5. Impedance spectra of DSCs in the dark condition ((a) Nyquist plot, (b) Bode plot) with bias potential of -0.68 V. Photoanodes with only N719 (the closed squares) and with F-SAM coadsorbent (the open circles), respectively.

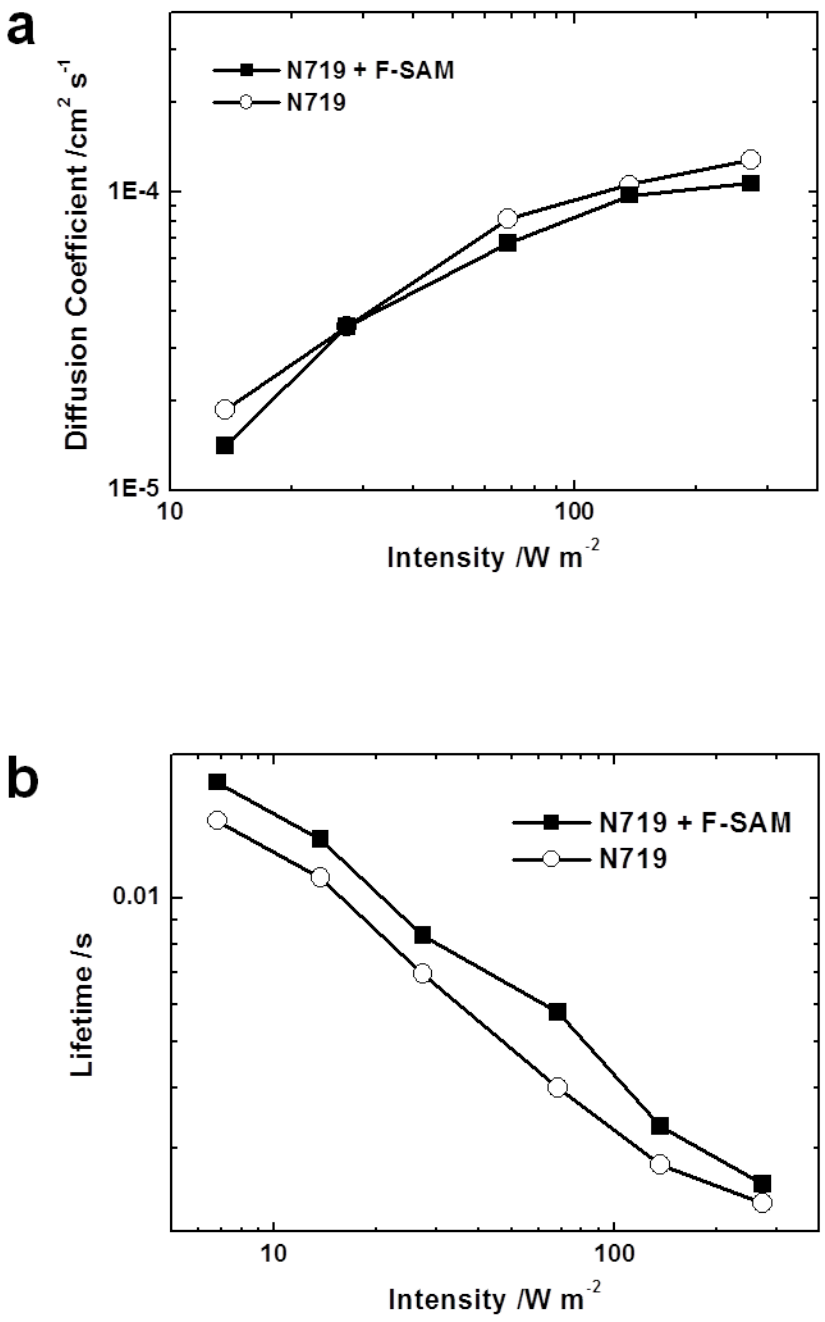

Figure 1.6. (a) The electron lifetime and electron diffusion coefficient determined by IMVS and IMPS as a function of light intensity.

1.3.3 Effect of Fluorinated Surface with Organic MK-2 Dye on the Photovoltaic Performance of DSCs

MK-2 organic dyes which give a high performance of incident photon-to-current conversion efficiency in a wavelength from 400 nm to 800 nm with a good long-term stability were characterized with fluorinated passivation layer. The photocurrent-voltage characteristics of DSCs with fluorinated passivation layer formed MK-2 dye sensitized photoanodes were measured under 1 Sun illumination with shading masks (active area: 0.25 cm^2) (Figure 1.7 a, b). Similar tendency with N719 dye sensitized photoanodes was observed. The photocurrent and the open-circuit voltage of photoanode with F-SAM were enhanced compare with only MK-2 dye sensitized photoanode, 10.8 mA cm^{-2} → 12.5 mA cm^{-2}, and 0.703 mV → 0.73 mV respectively (in table 1.2). It presents that the fluorinated monolayer also efficiently blocks the recombination in the interface between the electrolyte and the photoanodes sensitizing MK-2 organic dye.

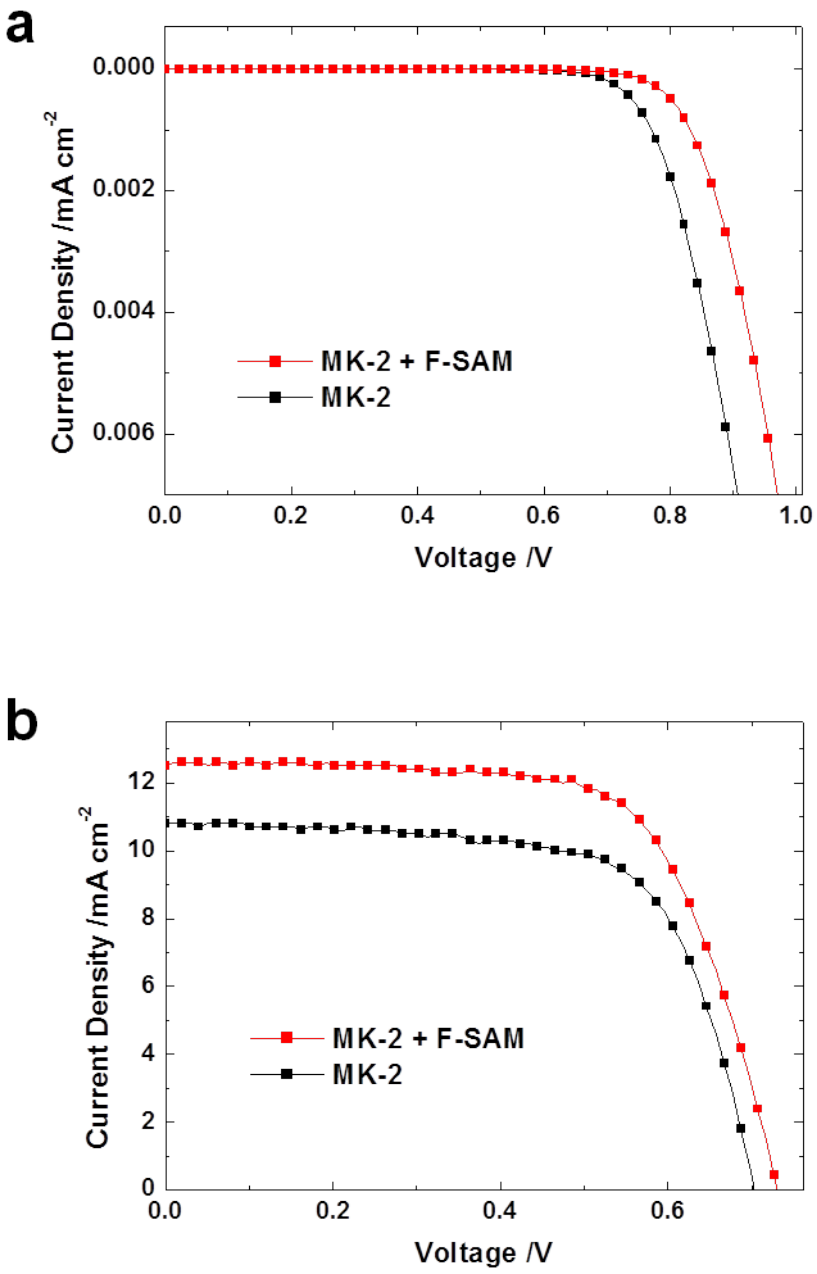

Figure 1.7. Photocurrent-voltage characteristics of DSCs sensitized with MK-2 and MK-2 / F-SAM (a, at dark condition and b, under illumination).

Table 1.2. I-V characteristics of the DSCs with MK-2 organic dye sensitized TiO_2 photoelectrodes employing CDCA and F-SAM coadsorbent

Type of TiO_2 electrode	V_{OC} (mV)	J_{SC} (mA cm^{-2})	FF (%)	Efficiency (%)
MK-2	**0.703**	**10.8**	**67.6**	**5.16**
MK-2 / CDCA	**0.686**	**11.6**	**72.1**	**5.72**
MK-2 / F-SAM	**0.731**	**12.5**	**67.7**	**6.19**
MK-2 / CDCA / F-SAM	**0.727**	**12.8**	**72.1**	**6.70**

1.3.4 Strategy for Secondary Coadsorbent on DSCs

The chenodeoxycholic acid (CDCA) is a well known coadsorbent for preventing aggregation of organic dye, such as MK-2 dye. These days, issue on organic dye has been aggregation of dye molecules on the TiO_2, causing electron quenching and lower photocurrent. When dye adsorbing process with dye and CDCA coadsorbent mixed solution, CDCA coadsorbent alleviate aggregation of dyes efficiently.

The CDCA molecules have low solubility with hexane like dye molecules. With these characteristics, in this study, we suggest a novel concept, a secondary passivation. First passivation of TiO_2 surface is performed with CDCA molecules, reducing aggregation. After dye and CDCA adsorption, fluorinated surface can be formed by sequential dipping process with F-SAM solution, named secondary passivation. This secondary passivation is expected for getting integration effect of dye aggregation and reduction of recombination.

In Figure 1.8, MK-2 and CDCA coadsorbed photoanode shows enhanced fill factor and photocurrent. Especially, fill factor is remarkably increased because of reduced aggregation of MK-2 dye molecules (Table 1. 2). After secondary passivation of MK-2 / CDCA coadsorbed TiO_2 surface with F-SAM solution, photocurrent and open-circuit voltage indicates even higher values comparing CDCA passivated photoanode. Though CDCA and MK-2 dyes adsorbed on the TiO2 surface, F-SAM can be formed on the bare site of TiO_2 and passivate more compactly. It presents successful combination of effects of

reduced aggregation by CDCA coadsorbent and decreased recombination by fluorinated passivation layer. Electrochemical impedance spectroscopy (EIS) measurement was performed in the dark with - 0.68 V of bias potential for quantitative analysis (Figure 1.8). In Figure 1.8 a, c, the Nyquist plots, the recombination resistances (R_{rec}) of TiO_2 photoanodes employing fluorinated monolayer are remarkably increased, in both case of with and without CDCA, comparing the value from photoanodes with only MK-2 dyes. For Bode plots in the dark (Figure 1.8 b, d), the characteristic frequency peak in the mid-frequencies (1 k - 10 Hz) of F-SAM formed photoanode is shifted to lower frequency, indicating the longer electron lifetime. From these results, we can notice that secondary passivation with F-SAM strategy is well established to get higher power conversion efficiency of DSCs by combining effect of both two coadsorbents.

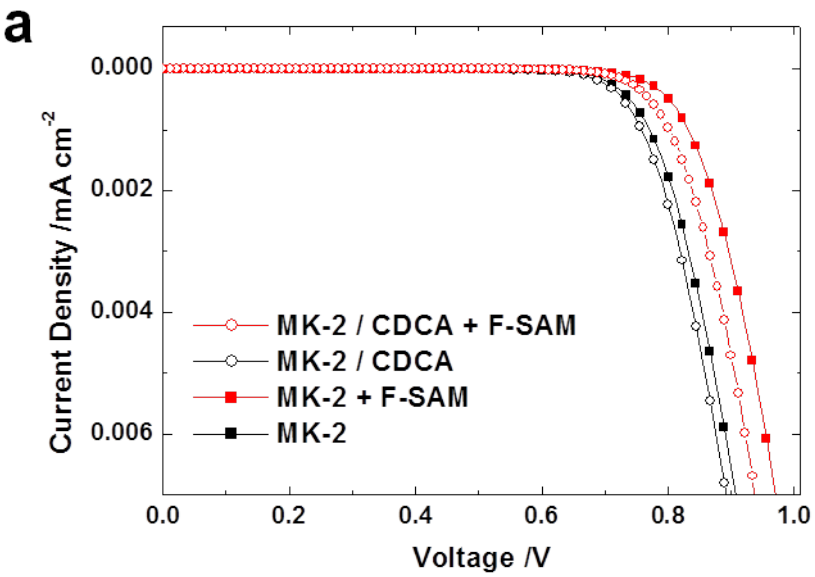
a
0.000
0.002
0.004
0.006
Current Density /mA cm-2
0.0
0.2
0.4
0.6
0.8
1.0
Voltage /V
MK-2 / CDCA + F-SAM
MK-2 / CDCA
MK-2 + F-SAM
MK-2

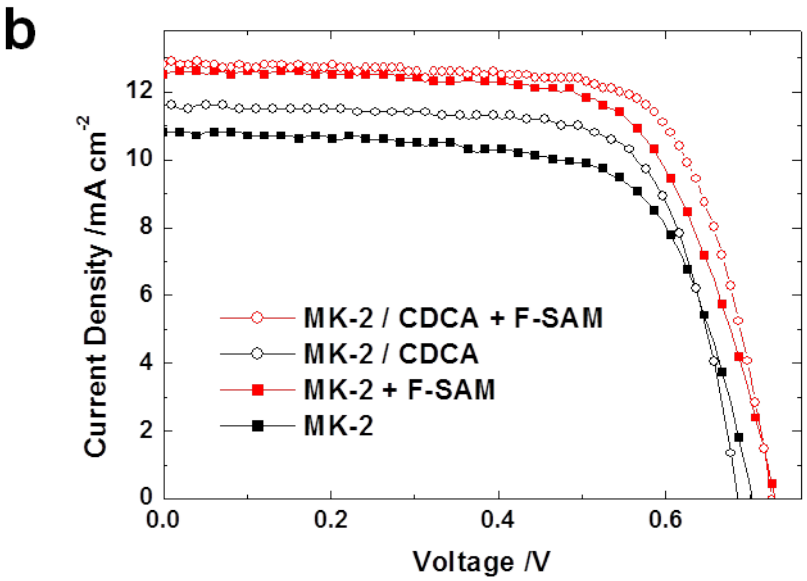
b
0
2
4
6
8
10
12
Current Density /mA cm-2
0.0
0.2
0.4
0.6
Voltage /V
MK-2 / CDCA + F-SAM
MK-2 / CDCA
MK-2 + F-SAM
MK-2

Figure 1.8. Photocurrent-voltage characteristics of DSCs sensitized with MK-2, MK-2 /CDCA, MK-2 / F-SAM and MK-2 / CDCA / F-SAM (a, at dark condition and b, under illumination).

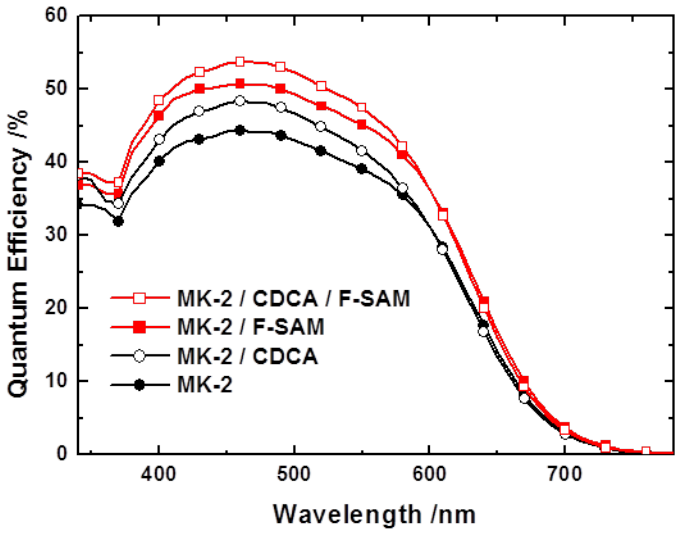

Figure 1.9. The external quantum efficiency of DSCs with MK-2, MK-2 /CDCA, MK-2 / F-SAM and MK-2 / CDCA / F-SAM, characterized by incident photon-to-current efficiency measurement.

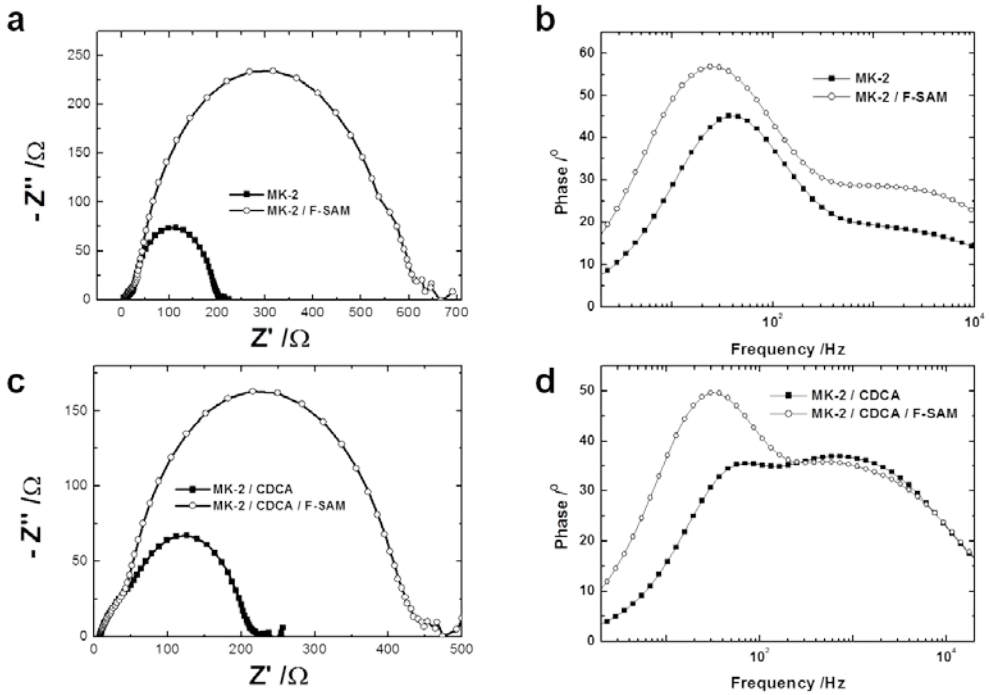

Figure 1.10. Impedance spectra of DSCs in the dark condition ((a), (c) Nyquist plot, (b), (d) Bode plot) with bias potential of -0.68 V. The photoanodes adsorbed with MK-2 solution ((a), (b)) and MK-2 / CDCA mixture solution ((c), (d)), without (the closed squares) and with F-SAM coadsorbent (the open circles), respectively.

1.4 Conclusion

In this study, the TiO_2 surface passivation with superhydrophobic surface on DSCs was demonstrated. Dye sensitizers were adsorbed on the TiO_2 structures by dip coating, fabricating photoanodes. After dye adsorption, uncovered TiO_2 surfaces were filled with 1H,1H,2H,2H-perfluorooctyltriethoxysilane by sequential adsorption process, as coadsorbents. With this novel method, fluorinate surfaces which have low surface energy were developed with compact monolayer and played an essential role in blocking layer of back electron reaction in the interface between TiO_2 and electrolyte, called electron recombination. We have analyzed the effects of the fluorinate surface on photovoltaic and electrochemical properties. The charge transfer resistance was remarkably increased by effective TiO_2 surface passivation, resulting in efficient block the electron recombination and enhanced photocurrent as well as photovoltage. Furthermore, in case of adsorbing organic dyes, coadsorbent prevented aggregation of dyes efficiently and induced considerable enhancement of electron injection into the TiO_2 photoanodes.

1.5 References

(1) O'Regan, B.; Grätzel, M. Nature **1991**, *353*, 737.

(2) Grätzel, M. Nature, **2001**, *414*, 338.

(3) Nazeeruddin, M. K.; Angelis, F. D.; Fantacci, S.; Selloni, A.; Viscardi, G.; Liska, P.; Ito S.; Takeru, B.; Grätzel, M. J. Am. Chem. Soc. **2005**, *127*, 16835.

(4) Yella, A.; Lee, H.-W.; Tsao, H. N.; Yi, C; Chandiran, A. K.; Nazeeruddin M. K.; Diau, E. W.-G.; Yeh, C.-Y.; Zakeeruddin, S. M.; Grätzel, M. Science **2011**, *334*, 629.

(5) Lee, S.-H. A; Abrams, N. M.; Hoertz, P. G.; Barber, G. D.; Halaoui, L. I. ;Mallouk, T. E. J. Phys. Chem. B **2008**, *112*, 14415.

(6) Wang, P.; Zakeeruddin, S. M.; Humphry-Baker, R.; Grätzel, M. Chem. Mater. **2004**, *162*, 694.

(7) Yum, J.-H.; Baranoff, E.; Wenger, S.; Nazeeruddin, M. K.; Grätzel, M. Energy Environ. Sci. **2011**, *4*, 842.

(8) Yum, J.-H.; Jang, S.-R.; Walter, P.; Geiger, T.; Nüesch, F.; Kim, S.; Ko, J; Grätzel, M.; Nazeeruddin, M. K. Chem. Commun. **2007**, 4680.

(9) Wang, P.; Zakeeruddin, S. M.; Humphry-Baker, R.; Moser, J. E.; Grätzel, M. Adv. Mater. **2003**, *15*, 2101.

(10) Zhang, Z.; Evans, N.; Zakeeruddin, S. M.; Humphry-Baker, R.; Grätzel, M. J. Phys. Chem. B **2003**, *107*, 14336.

(11) Gao, F.; Wang, Y.; Shi, D.; Zhang, J.; Wang, M.; Jing, X.; Humphry-Baker, R.; Wang, P.; Zakeeruddin, S. M.; Grätzel, M. J. Am. Chem. Soc. **2005**, *130*,

10720.

(12) Zhang, Z.; Evans, N.; Zakeeruddin, S. M.; Humphry-Baker, R.; Grätzel, M. J. Phys. Chem. C **2007**, *111*, 398.

(13) Han, L.; Islam, A.; Chen, H.; Malapaka, C.; Chiranjeevi, B.; Zhang, S.; Yang, X.; Yanagida, M. Energy & Environ. Sci. **2011**, *5*, 6057.

(14) Lee, Y.-G.; Park, S.; Cho, W.; Son, T.; Sudhagar, P.; Jung, J. H.; Wooh, S.; Char, K.; Kang, Y. S. J. Phys. Chem. B **2012**, *116*, 6770.

(15) Feldt, S. M.; Cappel, U. B.; Johansson, E. M. J.; Boschloo, G.; Hagfeldt, A. J. Phys. Chem. C **2010**, *114*, 10551.

(16) Shin, B.; Won, J.; Son, T.; Kang, Y. S.; Kim, C. K. Chem. Commun. **2010**, *47*, 1734.

(17) Wang, Z.-S.; Cui, Y.; Dan-oh, Y.; Kasada, C.; Shinpo, A.; Hara, K. J. Phys. Chem. C **2007**, *111*, 7224.

(18) Wang, M.; Grätzel, C.; Moon, S.-J.; Humphry-Baker, R.; Rossier-Item, N.; Zakeeruddin, S. M.; Grätzel, M. Adv. Funct. Mater. **2009**, *19*, 2163.

(19) Yum, J. H.; Moon, S. J.; Humphry-Baker, R.; Walter, P.; Geiger, T.; Nuesch, F.; Grätzel, M.; Zakeeruddin, S. M. Nanotechnology **2008**, *19*, 424005.

(20) Sugihara, H.; Wang, Z.-S. Langmuir **2006**, *22*, 9718.

(21) Lim, J.; Kwon, Y. S.; Park, S.-H.; Song, I. Y.; Choi, J.; Park, T. Langmuir **2011**, *27*, 14647.

(22) Neale, N. R.; Kopidakis, N.; Lagemaat, J.; Grätzel, M.; Frank, A. J. J. Phys. Chem. B **2005**, *109*, 23183.

(23) Deng, X.; Mammen, L.; Butt, H.-J.; Vollmer, D. Science **2012**, *335*, 67.

(24) Kang, S. M.; Kim, S. M.; Kim, H. N.; Kwak, M. K.; Tahk, D. H., Suh, K. Y. Soft Matter **2012**, *8*, 8563.

(25) Cheng, Y. T.; Rodak, D. E.; Wong, C. A.; Hayden, C. A. Nanotechnology **2006**, *17*, 1359.

(26) Tuteja, A.; Choi, W.; Mabry, J. M.; Mckinley, G. H.; Cohen, R. E. PNAS **2008**, *105*, 18200.

(27) Chang, B.; Sariola, V.; Aura, S.; Ras, R. H. A.; Klonner, M.; Lipsanen, H.; Zhou, Q. Appl. Phys. Lett. **2011**, *99*, 034104.

(28) Zisman, W. A. *Contact Angle, Wettability and Adhesion*, Advances in Chemistry Series 43, Am. Chem. soc.: Washingtion DC, **1964**.

(29) Kopidakis, N.; Neale, N. R.; Frank, A. J. J. Phys. Chem. B **2006**, *110*, 12485.

(30) Zhang, Z.; Zakeeruddin, S. M.; O'Regan, B. C.; Humphry-Baker, R.; Grätzel, M. J. Phys. Chem. B **2005**, *109*, 21818.

Chapter 2. Plasmon-Enhanced Photocurrent in Quasi-Solid-State Dye-Sensitized Solar Cells by the Inclusion of Gold / Silica Core-Shell Nanoparticles into TiO_2 Photoanode

2.1 Introduction

Dye-sensitized solar cells (DSCs) have currently received much attention due to several advantages such as low-cost of fabrication and high power conversion efficiency over 12 % under 1 sun illumination condition.[1-4] Most widely studied DSC comprises an electrolyte sandwiched structure between two transparent electrodes, photoanode and counter electrode. The photoanode consists of mesoporous semiconductor, e.g. TiO_2 layer with sensitizers, whereas a typical counter electrode is made of reduction catalyst such as platinum coated on a transparent conducting glass such as fluorine-doped tin oxide (FTO) glass. On exposing to light, the dye sensitizers adsorbed onto the surface of the mesoporous TiO_2 layer generate electrons which are injected into the TiO_2 layer for electricity production. Therefore, light harvesting by sensitizers on the photoanodes undoubtedly plays a major role in DSCs. A large number of researches have been working to enhance the light harvesting efficiency in the TiO_2 photoanodes. Among many others, one common approach is to utilize the new photoanode architecture e.g. introduction of scattering layer formation and

inverse opal nanostructures.[5-7] In addition, energy relay dyes,[8] organic dyes with higher extinction coefficient,[9,10] the cocktail system,[11,12] and the selective dyes adsorption techniques have been intensively investigated.[13,14]

The localized surface plasmon resonance (LSPR) phenomena of metal nanoparticles is also paid much attention to enhance light harvesting efficiency.[15-19] The LSPR which refers to the resonance between electromagnetic field and free-electron oscillation amplifies the electromagnetic field near the metal nanoparticles. This local field enhancement by direct coupling of LSPR affects efficient absorption of dye sensitizers and increases charge carrier generation in DSCs.[20-22] Recently, plasmon enhanced light harvesting as well as photocurrent generation were demonstrated with silver nanoparticles using the flat TiO_2 film as a photoanode.[23,24] The intense electromagnetic field by the LSPR affecting on dye molecules was verified with UV/Vis absorption spectra, and it showed a considerable theoretical promise in DSCs, despite low photocurrent and power conversion efficiency of devices due to absorbing light by a dye monolayer alone (14.6 μA cm^{-2} → 85.7 μA cm^{-2}, 0.007 %→ 0.045 %). To evaluate the effect of added LSPR structures, arrays of aligned elliptical Au disks were introduced on the flat TiO_2 layer.[25] It was useful starting point for investigating LSPR enhanced charge carrier generation and its mechanism by the near-field enhancement of elliptical Au disk. In addition, the methods for employing Au NPs in solid-state DSCs were introduced, spin-coating of Au NPs on the top surface of mesoporous TiO_2 layer.[26] From the spin-coating method, plasmonic enhanced charge carrier generation was realized and it was the first attempt to apply the LSPR in

conventional structure of DSCs.

For fabricating DSCs with metal nanoparticles in the presence of halide ions, such as I^- / I_3^-, based liquid type electrolyte, the stability of metal nanoparticles has been a major concern because halide ions can easily dissolve noble metals, for instance gold and silver, following chemical reaction.[27]

$$2\,Au + I_3^- + I^- \rightleftharpoons 2\,[AuI_2]^- \quad (1)$$

Due to this corrosion problem, core-shell structures of metal nanoparticles are necessary to apply LSPR in conventional DSCs. In this article, the gold/silica core-shell nanoparticles (Au@SiO_2 NPs), synthesized in solution process, are employed. The SiO_2 shells cover Au NPs homogeneously with thin (~10 nm) layers and prevent direct contact between Au NPs and I^- / I_3^- electrolyte. Moreover SiO_2 shells, which act as insulator from the electrolyte and the semi-conducting materials, inhibit the charge carrier recombination in the photoanode effectively.

As-synthesized Au@SiO_2 NPs were mixed with TiO_2 paste and incorporated into the mesoporous TiO_2 layer after sintering. This incorporation method of Au@SiO_2 NPs into the TiO_2 layer influence the effect of LSPR in a whole part of photoanodes overcoming the limitation of spin-coating method which affects only near the top surface and have no influence in the bulk of photoanodes. In addition, we introduce a novel approach called, corrosion treatment of Au cores fabricating the SiO_2 hollow spheres to verify the LSPR effect on the Au@SiO_2 NPs incorporated photoanodes. The core-shell nanoparticles incorporating photoanodes are affected by both metal cores and

shells. Even though a number of researches about improved photovoltaic characteristics by LSPR effect have been presented using metal / TiO_2 or SiO_2 core-shell structures, the quantitative analyses of the LSPR by metal cores and other changes in photoanodes by shells are still hard to evaluate separately. [23-24, 26] In this context, the SiO_2 hollow spheres realize definitely the same morphology with TiO_2 photoanodes incorporating Au@SiO_2 NPs and help for accurate comparison of photoanodes with and without LSPR. From this approach, we demonstrate the recent issue of the LSPR effect in DSCs independently with effect of SiO_2 shells such as the charge injection problem from dyes onto the SiO_2 shell and the change of morphology and resistances.

2.2 Experimental Section

2.2.1 Materials

All chemicals were used without any further purification and water was always doubly ionized. Chemicals used for the synthesis of Au@SiO_2 NPs, hydrogen tetrachloroaurate (III) trihydrate ($HAuCl_4$ • 3 H_2O), Hexadecyltrimethylammonium bromide ($CH_3(CH_2)_{15}N(Br)(CH_3)_3$), sodium citrate ($HOC(COONa)(CH_2COONa)_2$ • 2 H_2O), ascorbic acid ($C_6H_8O_6$), (3-Mercaptopropyl) trimethoxysilane ($HS(CH_2)_3Si(OCH_3)_3$) and sodium silicate solution ($Na_2O(SiO_2)x$ • xH_2O) were purchased from Sigma Aldrich. For the fabrication of the dye sensitized solar cells, polyethyleneglycol dimethylehter (PEGDME, Mw: 500), 1-methyl-3-propylimidazoliumiodide (MPII), iodine (I_2) and fumed silica (~14 nm) were obtained from Sigma-Aldrich whereas TiO_2 paste (DSL 18NR-T) and dye as a sensitizer, *cis*-diithiocyanato-bis(2,2'-bipyridyl-4,4'-dicarboxylato)-ruthenium(II) bis(tetrabutylammonium), so called N719 were purchased from Dyesol.

2.2.2 Synthesis of gold nanoparticles

Au NPs were prepared using a seed-mediated method.[22] First, 15 nm diameter Au NPs as seeds were synthesized via citrate reduction. In a typical procedure, 10 ml of 1 mM gold (III) chloride trihydrate aqueous solution was refluxed at boiling temperature under vigorous stirring, followed by the quick injection of 1 ml of 39 mM sodium citrate solution. After 15 min heating was

stopped and reaction contents were cool down to room temperature to work it up. To make the larger size of nanoparticles, 2 ml seed particle solution was added into 100 ml of 0.5 mM gold (III) chloride trihydrate aqueous solution containing 0.03 M CTAB and 1 mM ascorbic acid. It was reacted for 4 hours and product was collected using centrifugation (9,000 rpm, at room temperature for 10 min).

2.2.3 Synthesis of gold / silica core-shell nanoparticles

Au@SiO_2 NPs were synthesized by a modified procedure previously reported by R. Corn.[23] In this method, growth of silica was performed after surfactant substitution with silane coupling group, (3-mercaptopropyl) trimethoxysilane (MPTMS). MPTMS in ethanol was added in the Au NPs solution. After 3 hours, sodium silicate aqueous solution was added and made to react for further 3 days. The contents were purified by several times precipitation using centrifugation and finally were re-dispersed in ethanol.

2.2.4 Paste preparation

As-prepared Au@SiO_2 NPs dispersed in ethanol solution were added and well mixed into the commercial titanium dioxide (TiO_2) paste with average size of 20 nm (DSL 18NR-T, Dyesol). In order to achieve the same thickness of photoanodes after sintering process, the excess of ethanol from the paste was evaporated using nitrogen stream to get homogenous concentration of paste materials.

2.2.5 Device fabrication

0.1 M of Ti (IV) bis(ethyl acetoacetato)-diisopropoxide in 1-butanol solution was spin-coated onto the FTO glass followed by sintering at 500 ºC for the formation of electron blocking layer between TCO substrate and oxidized species in the electrolyte. TiO_2 photoandes were fabricated by TiO_2 pastes as described above using doctor blade method onto the FTO substrate (TEC 8, Pilkington) and then sintered at 500 °C for 15 min. Subsequently, TiO_2 nanostructures coated FTO substrates were dipped into 40 mM $TiCl_4$ in H_2O solution at 70 °C for 30 min and sintered at 500 °C for 15 min.

TiO_2 electrodes were dipped into the 0.3 mM N719 dye (cis-bis(isothiocyanato)bis(2,2'-bipyridyl-4,4'-dicarboxylato)-ruthenium (II) bis-tetrabutylammonium, Dyesol) in the acetonitrile and tert-butanol solution (1:1 v/v) at 30 °C for 18 hours and then rinsed with acetonitrile and dried using stream of nitrogen. Pt counter electrode was prepared by thermal decomposition of 0.01 M H_2PtCl_6 in isopropylalcohol solution on the FTO substrate followed by sintering at 500 °C for 30 min. After loading the dyes onto the TiO_2 electrodes, Surlyn (25 μm, Solaronix) was attached on the TiO_2 working electrode as a spacer and the polymer electrolyte was spread on the gap of spacer, and then Pt counter electrode was placed on it.

The electrolyte consists of poly(ethylene glycol dimethyl ether) (PEGDME) (Mw: 500, Sigma-Aldrich), 1-methyl-3-propylimidazolium iodide (MPII, Sigma-Aldrich), iodine (I_2, Sigma-Aldrich), and fumed silica nanoparticles (14 nm, Sigma-Aldrich). The composition of [-O-]:[MPII]:[I_2] is

10:1:0.1 and the silica NPs are added 9 wt% of the total polymer electrolyte.[22]

2.2.6 Electron microscopy

The nanoparticles were characterized using transmission electron microscopy (TEM), JEM-2100 (JEOL) with an acceleration voltage of 200 kV. Field-emission scanning electron microscopy (FE-SEM) was performed using a JSM-5701F (JEOL).

2.2.7 Solar cell characterization

Thicknesses and absorption properties of photoanodes were characterized with surface profiler (alpha-step IQ, Tencor) and UV-Vis spectroscopy (V-670 UV-Vis spectrophotometer, Jasco), respectively. Current-voltage characterization of the DSCs was carried by a Keithley 2400 digital source meter and solar simulator equipped with 300 W Xenon arc-lamp (Newport) under 1 sun illumination (AM 1.5, 100 mW cm^{-2}). The light intensity was calibrated by silicon solar cell (PV measurement). In addition, quantum efficiency of DSCs was analyzed by incident photon to current efficiency (IPCE) (PV measurements, Inc.) as a function of wavelength. Charge transfer resistance and electron lifetime in photoanodes were characterized by electrochemical impedance spectroscopy (EIS) using IM6 (Zahner) under dark and illumination condition with bias potential of -0.54 V. The frequency was in the range of 1 M - 0.1 Hz and amplitude was fixed to 10 mV. The obtained spectra were fitted and analyzed using Z-View software with equivalent circuits.

The electron diffusion coefficient and electron lifetime in photoanodes were evaluated by intensity-modulated photocurrent spectroscopy (IMPS) under short-circuit conditions and intensity-modulated photovoltage spectroscopy (IMVS) under open-circuit conditions as a function of light intensity using a CIMPS (Controlled Intensity Modulated Photo Spectroscopy) system (Zahner) and white light source (Zahner). The detailed measurement conditions are described elsewhere.

2.3 Results and Discussion

2.3.1 Fabrication of Gold / Silica Core-Shell Nanoparticles Incorporated Photoanodes for DSCs

Figure 2.1 a-c show TEM images of the Au NPs with three different sizes covered with SiO_2 shell. Initially, Au NPs with average diameters of (a) 30, (b) 50, and (c) 160 nm were synthesized by varying the concentration of the Au precursor. Subsequently their surfaces were modified with 3-mercaptopropyl trimethoxysilane (MPTMS), and the thickness of SiO_2 shells were controlled to be around 11 nm by adding an aqueous solution of sodium silicate.

Even though the Au NPs were protected by SiO_2 shell (Au@SiO_2 NPs), the Au cores were still able be corroded by the penetration of liquid electrolytes (I^- / I_3^- ions) through the small pinholes of the silica shell in a few hours. Therefore, the SiO_2 shell was treated with $TiCl_4$ to block the pinholes and subsequently to improve the stability against corrosion by iodine. In addition, a poly(ethylene glycol)dimethylether (PEGDME, Mw: 500) based polymer electrolyte, instead of typical acetonitrile based liquid electrolytes, is used as a matrix for quasi-solid-state DSCs to overcome the penetration of electrolytes through the pinholes.

The effect of the localized surface plasmon resonance (LSPR) decreases exponentially to the distance between NPs and dyes. However, based on our experimental results, the SiO_2 shell thinner than 8 nm in thickness hardly

protected Au core from the electrolyte penetration, even though PEGDME was applied as matrix of electrolyte. Experimental facts show that, 10 nm was the minimum thickness of the SiO_2 shell to protect Au core from corrosion.

The plasmonic absorption bands of Au@SiO_2 NPs with different size of Au core were characterized using UV-Vis spectroscopy. As shown in Figure 2.1 d, the absorption peaks appear at 537, 547, and 565 nm for Au@SiO_2 NPs with size of Au core/SiO_2 shell 30/12, 50/11, and 160/10 nm, respectively. This shift in the absorption band is attributed to the change in the oscillation frequency of LSPR by varying average diameter of Au NPs. The absorption band of LSPR moves to longer wavelength by increasing the size of Au NPs, as a result of decrease in the oscillation frequency.[23,24] The coupling between the LSPR of Au NPs and the absorption of dyes is one of the key factor for enhanced performance of DSCs using Au NPs. In our case, the absorption peak difference of Au NPs (160 nm) with respect to the N719 dyes was ~ 40 nm, as shown in Figure 2.1 d. Additionally, when the larger Au NPs are incorporated into the TiO_2 photoanodes, the surface area of the photoanodes becomes smaller which reduces the dye loading capacity, resulting in the decrease of photocurrent in DSCs. On the contrary, as the size of the Au NPs increases, the field enhancement is more widely developed, leading to the increased light harvesting of dyes.[23,24] Considering above all factors, such as the coupling wavelength mismatch, the change of surface area, and the near-field enhancement effects, 50/11 nm Au@SiO_2 NPs were chosen for fabrication of photoanodes to investigate the effects of LSPR in DSCs.

Figure 2.2 a shows the schematic illustration of $Au@SiO_2$ NPs incorporated TiO_2 photoanode in DSC. The LSPR of $Au@SiO_2$ NPs in TiO_2 photoanodes was indicated by the photograph showing reddish colored photoanode and confirmed by UV-Vis spectrum with absorption band as shown in Figure 2.2 b. Figure 2.2 c shows $Au@SiO_2$ NPs in the photoanodes surrounded by TiO_2 NPs using scanning electron microscopy (SEM), and it is noticed that the shape of the $Au@SiO_2$ NPs are still unchanged after sintering at 500 °C.

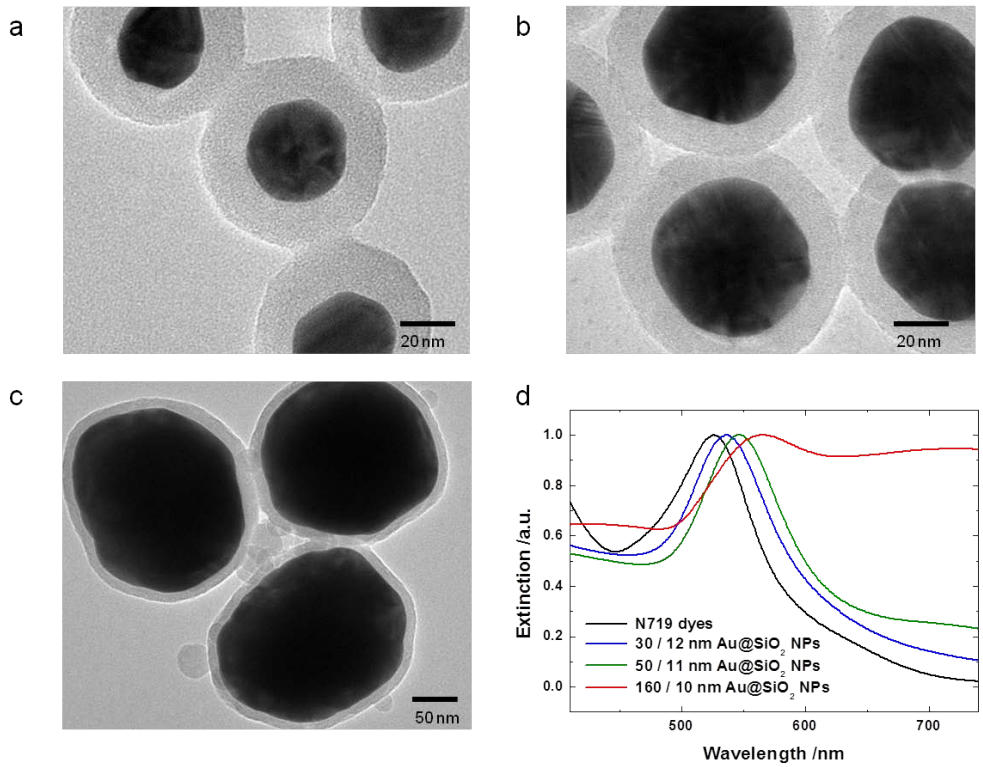

Figure 2.1. Transmission electron spectroscopy (TEM) of various size of $Au@SiO_2$ NPs, (a) 30 / 12 nm, (b) 50 / 11 nm, and (c) 160 / 10 nm. (d) Normalized UV-Vis spectrum of the N719 dyes and the $Au@SiO_2$ NPs in ethanol.

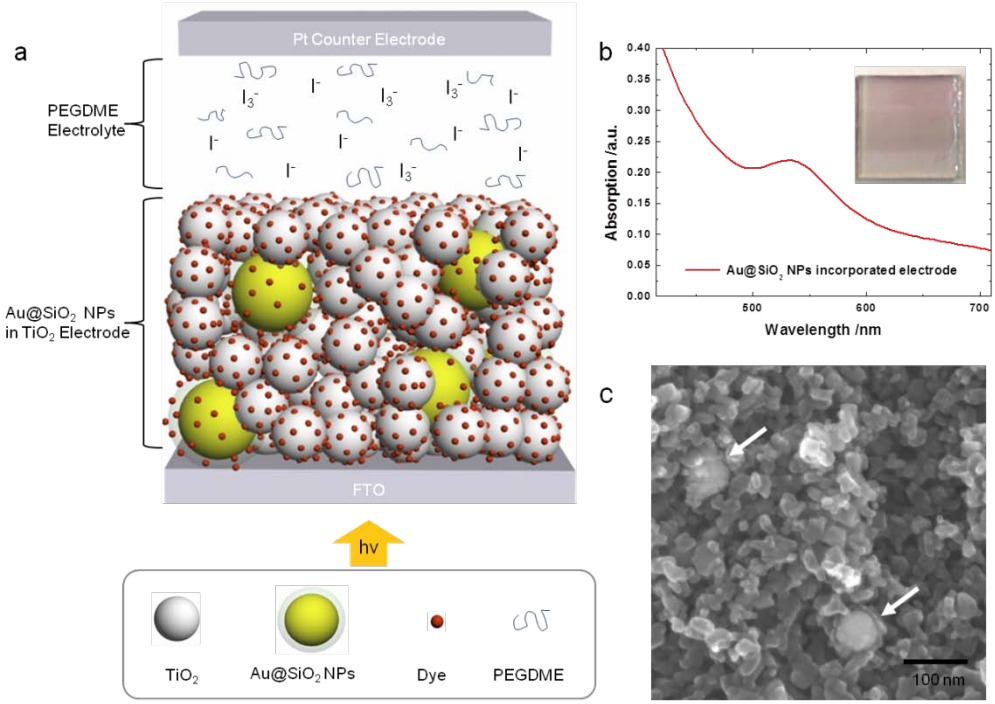

Figure 2.2. (a) Schematic illustration of $Au@SiO_2$ NPs incorporated photoanode in PEGDME based quasi-solid-state DSC. (b) UV-Vis spectrum and photograph and (c) cross sectional scanning electron microscopy (SEM) image of $Au@SiO_2$ NPs incorporated photoanode with an diameter of ~ 20 nm of TiO_2 nanoparticles (white arrows indicate $Au@SiO_2$ NPs).

2.3.2 Photocurrent-Voltage Characteristics of DSCs with $Au@SiO_2$ NP Incorporated Photoanodes.

The photocurrent-voltage characteristics of DSCs with TiO_2 photoanodes employing $Au@SiO_2$ NPs are represented in Figure 2.3. The film thickness of photoanodes with and without $Au@SiO_2$ NPs was adjusted at 2 μm, thinner than conventional TiO_2 layer, [25] to characterize effect of LSPR definitely. In order to optimize the incorporation method of $Au@SiO_2$ NPs for DSC performance, the concentration of $Au@SiO_2$ NPs in TiO_2 paste was varied from 0.25 to 1.5 wt%. The short circuit current density (Jsc) is increased upon the incorporation of $Au@SiO_2$ NPs, while the open-circuit voltage (Voc) and fill factor (FF) nearly remain the same. The Jsc and power conversion efficiency (PCE) of photoanodes with addition of 1.0 wt% of $Au@SiO_2$ NPs were increased up to 5.67 mA cm^{-2} and 2.66 % respectively, which is over 30 % enhancement with respect to the same thickness of the reference TiO_2 photoanode without $Au@SiO_2$ NPs (4.35 mA cm^{-2}, 1.94 %). However, at concentrations higher than 1.0 wt% of $Au@SiO_2$ NPs, the Jsc (5.44 mA cm^{-2}) and PCE (2.53 %) were slightly decreased, as shown in Figure 2.3 (b) and Table 2.1.

From these results, we can suggest some possible side effects for the inclusion of $Au@SiO_2$ NPs for DSCs. First of all, it is expected that the total incident light is hindered by the absorption of $Au@SiO_2$ NPs in photoanodes which resulted in the reduction of light absorption of dyes.[18] Secondly, $Au@SiO_2$ NPs with size ~70 nm decrease total amount of dye loading in the photoanodes,

due to small surface area relative to TiO_2 NPs of 20 nm. Lastly, it is hard to inject electron from dyes onto the SiO_2 shell, as insulator, to the near TiO_2 NPs. These side effects of inclusion due to the Au@SiO_2 NPs may attribute to the decrease in both photocurrent and photovoltaic performance of DSCs to a small extent.

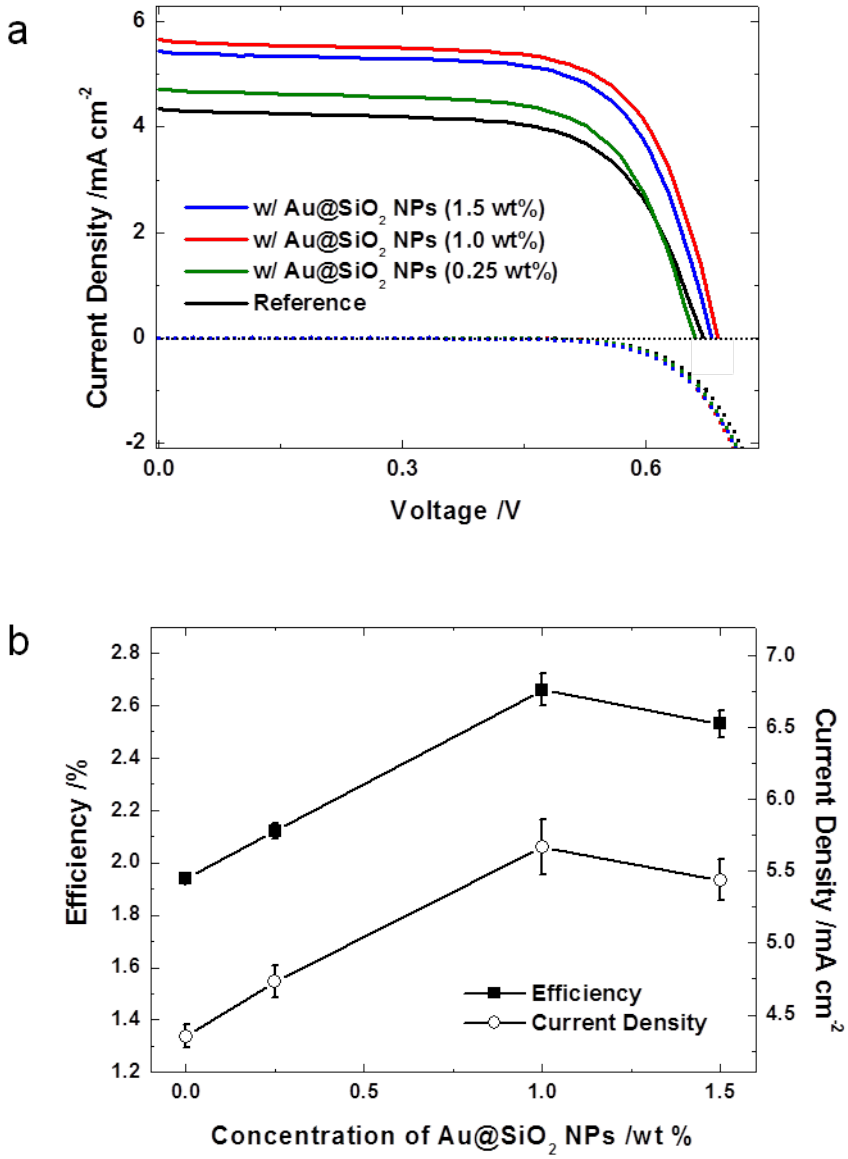

Figure 2.3. (a) Photocurrent-voltage characteristics of DSCs with different concentration of Au@SiO_2 NPs, under illumination (continuous line) and in dark (dot line). (b) Plot of power conversion efficiency (the closed squares) and short circuit current density (the open circles) versus concentration of Au@SiO_2 NPs.

Table 2.1. I-V characteristics of the DSCs with TiO_2 photoelectrodes employing $Au@SiO_2$ NPs and SiO_2 hollow spheres.[a]

Type of TiO_2 electrode	Concentration of $Au@SiO_2$ NPs (wt%)	V_{OC} (V)	J_{SC} (mA cm^{-2})	FF (%)	Efficiency (%)
Reference (only TiO_2)	-	0.664	4.35	67.0	1.94
w/ $Au@SiO_2$ NPs	0.25	0.657	4.73	67.8	2.12
	1.0	0.684	5.67	68.6	2.66
	1.5	0.676	5.44	68.7	2.53
w/ SiO_2 hollow spheres	1.5	0.665	4.4	67.7	1.97

[a] The thickness of TiO_2 photoanodes are adjusted with 2 μm; measured under 1 Sun condition (AM 1.5, 100 mW cm^{-2}) with 0.25 cm^2 active area.

2.3.3 Corrosion Treatment of Au Core For Fabricating Hollow Silica NPs

In order to evaluate the quantitative effect of LSPR from Au core and other changes from SiO_2 shell separately, the comparison of Au@SiO_2 NPs incorporated photoanodes with and without Au core is necessary. Here, we have introduced a novel approach for fabrication of SiO_2 hollow spheres by corrosion treatment. After dipping photoanodes incorporating Au@SiO_2 NPs into I^- / I_3^- liquid electrolyte, Au core was completely dissolved in few hours, as mentioned above. From this process, we realize the photoanodes with SiO_2 hollow sphere which have definitely same morphology and thickness of photoanodes incorporating Au@SiO_2 NPs. After fabricating SiO_2 hollow spheres, as expected that Au core was exclusively removed without any morphology change, which can be easily demonstrated by the disappearance of reddish color, as shown by photograph in Figure 2.4. UV-Vis spectra (Figure 2.5 a) indicate the disappearance of absorption band of Au@SiO_2 NPs which is a consequence of dissolving Au core. In addition, Figure 2.5 b shows the decreased light absorption of N719 dyes which are adsorbed onto TiO_2 photoanodes incorporating SiO_2 hollow spheres. The only difference between these photoanodes was existence of Au core, thus, it is reasonable evidence that the enhancement of light absorption is mainly attributed to the LSPR effect of Au core.

Figure 2.5 c shows the photocurrent-voltage (J-V) characteristics of DSCs, which are well consistent with the results obtained from difference in light absorption as shown in Figure 2.5 a and b. DSCs based on TiO_2 photoanode

incorporating Au@SiO_2 NPs exhibited ~ 30 % higher Jsc as well as PCE than those with SiO_2 hollow spheres. The increase of Jsc was found to agree well with the results from incident photon-to-current efficiency (IPCE) measurement and the difference obtained by subtracting IPCE values is well matched with absorption band of LSPR (Figure 2.5 d). Moreover, the photoanode incorporating SiO_2 hollow spheres shows similar Jsc of 4.4 mA cm^{-2} and PCE of 1.97 % with respect to reference TiO_2 photoanode, as summarized in Table 2.1. The photoanodes incorporating SiO_2 hollow spheres were removed only Au core, maintaining surface area and morphology of TiO_2 photoanode. Thus, from comparison of photovoltaic performance with reference and SiO_2 hollow spheres incorporated photoanodes, it was noted that a less change of surface area and morphology has occurred on inclusion of small amount (1.5 wt%) of Au@SiO_2 NPs into the TiO_2 photoanode, and we demonstrated experimentally that the light hindering effect of Au NPs was dominant among different side effects.

For further investigation of influence on interfacial charge transport properties, electrochemical impedance spectroscopy (EIS) measurement were performed in the dark (Figure 2.6 a and b) and under illumination (Figure 2.6 c and d) with bias potential (-0.54 V). Each result was fitted with general transmission model of DSCs, as shown in Figure 2.6 e.[26] The electron transport resistance, the electron recombination resistance, and the capacitance for DSCs are summarized in inset table of Figure 2.6 b and d. In Figure 2.6 a and c, the Nyquist plots show two predominant semicircles. The first semicircle at high frequency is attributed to the charge transfer resistance at the Pt counter

electrode/polymer electrolyte interface (R_{pt}) and the second one at mid-frequencies is associated with the electron transport (R_t) and the electron recombination (R_{rec}) at the TiO_2/polymer electrolyte interface.

The recombination resistances (R_{rec}) of TiO_2 photoanode employing Au@SiO_2 NPs are decreased with respect to SiO_2 hollow spheres, both in the dark and under illumination. In spite of the fact that Au core was surrounded with SiO_2 shell, it shows that Au NPs still act as the charge trap and the recombination site, making the recombination resistance lower. The capacitances in the dark are similar between both samples. However, under illumination, the capacitance of photoanode with Au@SiO_2 NPs is much higher than that of photoanode incorporating SiO_2 hollow spheres due to the enhanced charge generation, and it is the strong evidence of the enhanced light harvesting of dyes by the LSPR of Au NPs.[27,28]

For Bode plots in the dark and under illumination (Figure 2.6 b and d), the characteristic frequency peak in the mid-frequencies (1 k - 10 Hz) is unchanged, indicating the same electron lifetime between the two samples. In addition, the role of the Au@SiO_2 NPs in the electron lifetime and electron diffusion coefficient in TiO_2 photoanodes are also evaluated from incident-modulated photovoltage spectroscopy (IMVS) and incident-modulated photocurrent spectroscopy (IMPS) as a function of light intensity as given in Figure 2.7. In accordance with the results from EIS measurements (Bode plot, Figure 2.6 b and d), the electron lifetime upon the inclusion of Au@SiO_2 NPs is maintained constantly, compared to that of photoanode with SiO_2 hollow spheres.

It presents that Au NPs had no influence on the electron lifetime in photoanodes of DSCs. Furthermore, electron diffusion coefficient is also unchanged, thus, the diffusion length (L_n, $L_n = (D_n\tau_n)^{1/2}$) derived from these values are almost the same when we apply Au@SiO_2 NPs in TiO_2 photoanode.

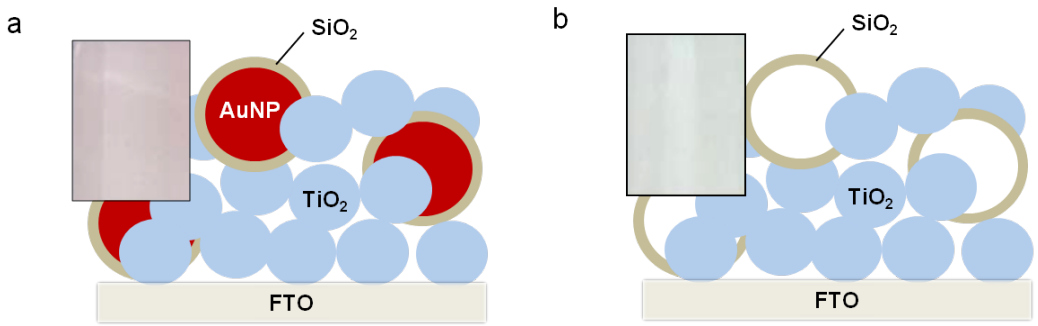

Figure 2.4. Schemes of TiO_2 photoanode incorporating (a) Au@SiO_2 NPs and (b) SiO_2 hollow spheres fabricated by corrosion treatment. Photographs of the corresponding electrodes are shown as insets.

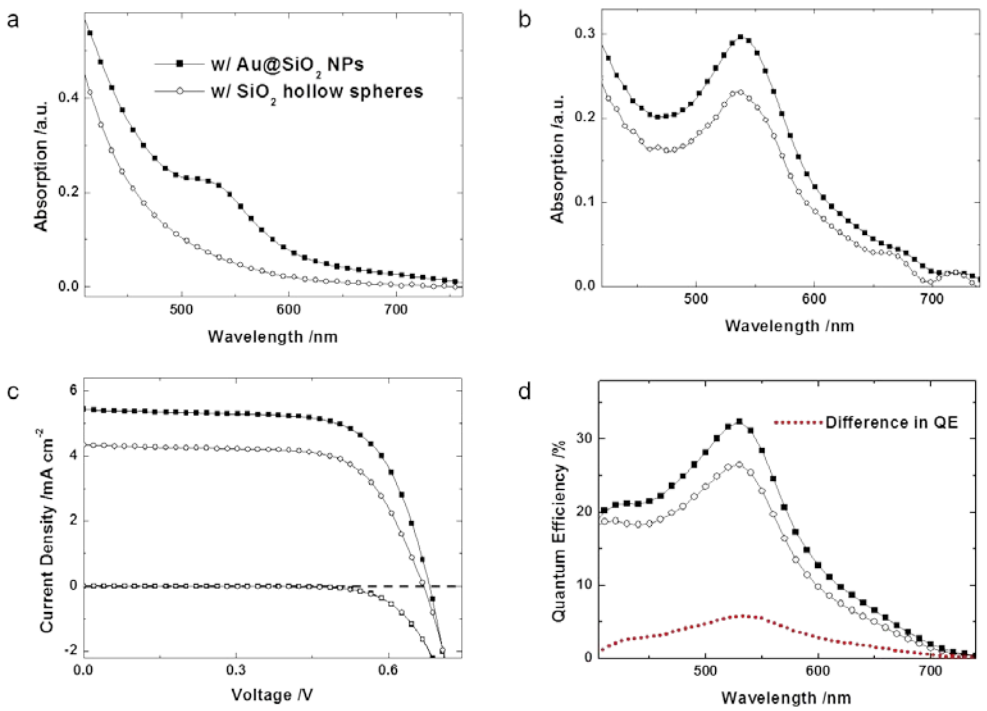

Figure 2.5. (a), (b) UV-visible spectroscopy, (c) Photocurrent-voltage characteristics and (d) IPCE spectrum of DSCs characterized with the inclusion of Au@SiO_2 NPs (the closed squares) and SiO_2 hollow spheres (the open circles). (a) Absorption spectrum of TiO_2 photooelectrodes without dyes and (b) with N719 dyes. Devices had 2 μm of the TiO_2 films and photovoltaic performance was measured under 1 sun condition (AM 1.5, 100 mW cm^{-2} solar illumination) with 0.25 cm^2 active area.

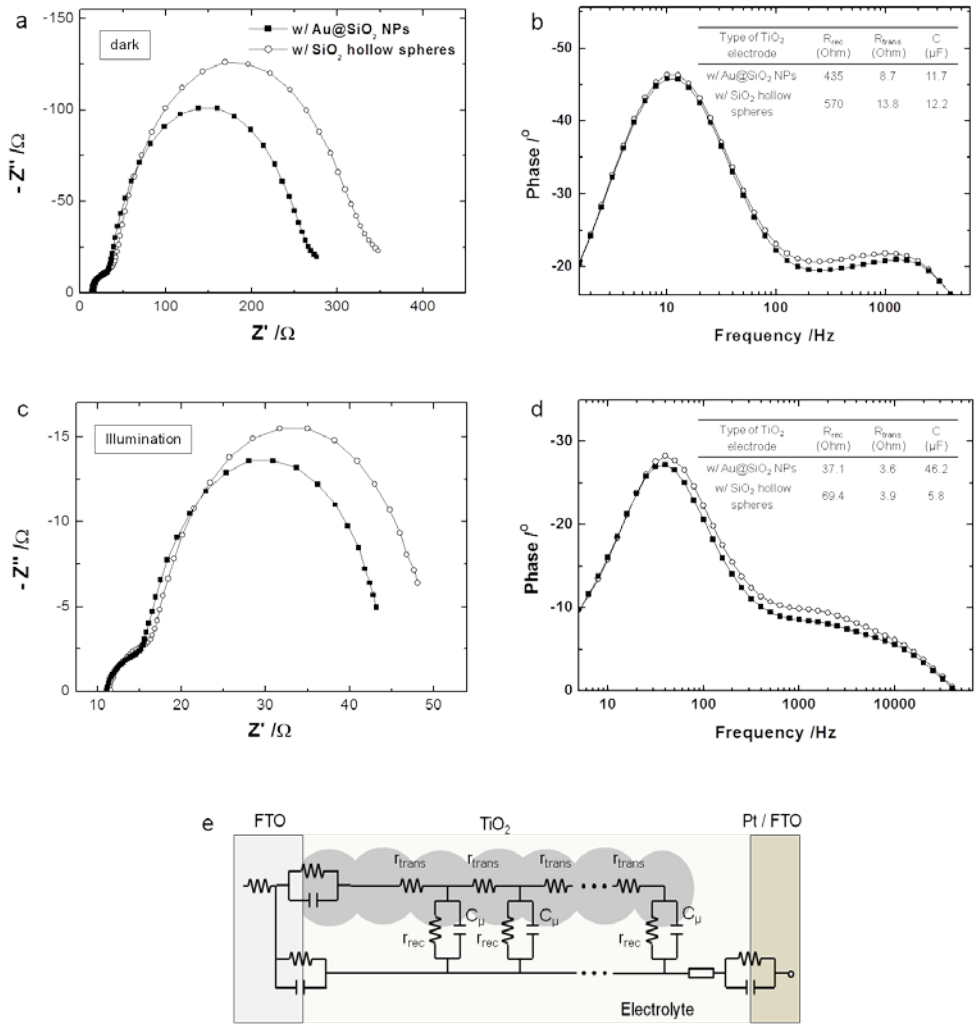

Figure 2.6. Impedance spectra of DSCs in the dark ((a) Nyquist plot, (b) Bode plot) and under illumination ((c) Nyquist plot, (d) Bode plot) condition with bias potential of -0.54 V. Photoanodes with $Au@SiO_2$ NPs (the closed squares) and with SiO_2 hollow spheres (the open circles), respectively. (e) General transmission line model of DSCs.[26]

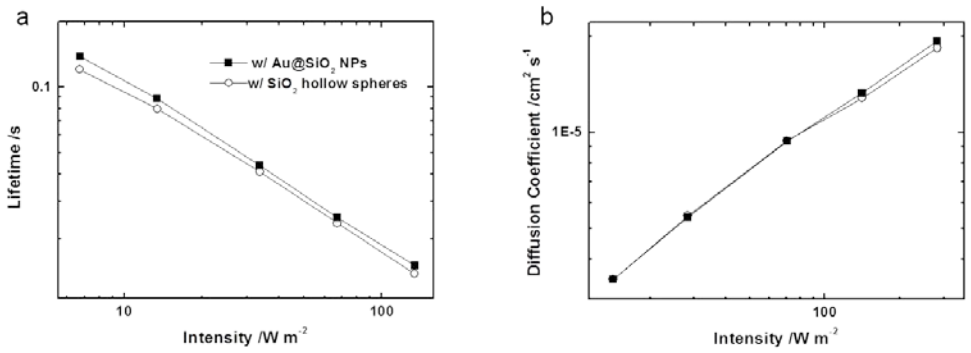

Figure 2.7. (a) The electron lifetime and (b) the electron diffusion coefficient determined by IMVS and IMPS as a function of light intensity, respectively.

2.4 Conclusion

In summary, we have reported the method to incorporate the $Au@SiO_2$ NPs into TiO_2 photoanodes and their effect on photovoltaic performance of DSCs with PEGDME electrolyte. $Au@SiO_2$ NPs increased the Jsc of DSCs up to 30 % from 4.35 mA cm^{-2} (w/o $Au@SiO_2$ NPs) to 5.67 mA cm^{-2} under 1 sun illumination condition. In addition, the SiO_2 hollow spheres were fabricated by corrosion treatment with I^- / I_3^- solution to eliminate Au core and make condition for accurate comparison between with and without Au NPs. Using this novel method, we have analyzed the effects of the $Au@SiO_2$ NPs on optical, electrochemical, and photovoltaic properties of the photoanodes. The influence from SiO_2 shell and morphology change were characterized separate from the influence from LSPR of Au core. From this, we demonstrated dominant side effect of incorporation of $Au@SiO_2$ NPs in DSCs, the hindering light effect by absorption of Au core. Lastly, it has been demonstrated with EIS measurement that the incorporation of $Au@SiO_2$ NPs affect the enhancement of light harvesting of dye molecules exclusively and following increases Jsc of DSCs without changing the electron lifetime and diffusion coefficient of TiO_2 photoanodes.

2.5 References

(1) O'Regan, B.; Grätzel, M. Nature **1991**, *353*, 737.

(2) Grätzel, M. Nature **2001**, *414*, 338.

(3) Nazeeruddin, M. K.; Angelis, F. D.; Fantacci, S.; Selloni, A.; Viscardi, G.; Liska, P.; Ito S.; Takeru, B.; Grätzel, M. J. Am. Chem. Soc. **2005**, *127*, 16835.

(4) Yella, A.; Lee, H.-W.; Tsao, H. N.; Yi, C; Chandiran, A. K.; Nazeeruddin M. K.; Diau, E. W.-G.; Yeh, C.-Y.; Zakeeruddin, S. M.; Grätzel, M. Science **2011**, *334*, 629.

(5) Hardin, B. E.; Hoke, E. T.; Armstrong, P. B.; Yum, J. H.; Comte, P.; Torres, T.; Frechet, J. M. J.; Nazeeruddin, M. K.; Grätzel, M.; McGehee, M. D. Nat. Photonics **2009**, *3*, 406.

(6) Chen, C.-Y.; Wang, M.; Li, J.-Y.; Pootrakulchote, N.; Alibabaei, L.; Ngoc-le, C.-H.; Decoppet, J.-D.; Tsai, J.-H.; Grätzel, C.; Wu, C.-G.; Zakeeruddin, S. M.; Grätzel, M. ACS Nano **2009**, *3*, 3103.

(7) Cai, N.; Moon, S.-J.; Cevey-Ha, L.; Moehl, T.; Humphry-Baker, R.; Wang, P.; Zakeeruddin, S. M.; Grätzel, M. Nano Lett. **2011**, *11*, 1452.

(8) W. Zhao, Y. J. Hou, X. S. Wang, B. W. Zhang, Y. Cao, R. Yang, W. B. Wang and X. R. Xiao, Sol. Energy Mater. Sol. Cells, **1999**, *58*, 173.

(9) Yum, J.-H.; Jang, S.-R.; Walter, P.; Geiger, T.; Nüesch, F.; Kim, S.; Ko, J; Grätzel, M.; Nazeeruddin, M. K. Chem. Commun. **2007**, 4680.

(10) Lee, K.; Park, S. W.; Ko, M. J.; Kim, K.; Park, N.-G. Nat. Mater., **2009**, *8*, 665.

(11) Yum, J.-H.; Baranoff, E.; Wenger, S.; Nazeeruddin, M. K.; Grätzel, M. Energy Environ. Sci. **2011**, *4*, 842.

(12) Subramanian, V.; Wolf, E.; Kamat, P. V. J. Phys. Chem. B **2001**, *105*, 11439.

(13) Tian, Y.; Tatsuma, T. J. Am. Chem. Soc. **2005**, *127*, 7632.

(14) Standridge, S. D.; Schatz, G. C,; Hupp, J. T. J. Am. Chem. Soc. **2009**, *131*, 8407.

(15) Standridge, S. D.; Schatz, G. C,; Hupp, J. T. Langmuir **2009**, *25*, 2596.

(16) Hägglund, C.; Zäch, M.; Kasemo, B.; Appl. Phys. Lett. **2008**, *92*, 013113.

(17) Brown, M. D.; Suteewong, T.; Kumar, R. S. S.; D'Innocenzo, V.; Petrozza, A.; Lee, M. M.; Wiesner, U.; Snaith, H. J. Nano Lett. **2011**, *11*, 438.

(18) Ding, B; Lee, B. J.; Yang, M.; Jung, H. S.; Lee, J.-K. Adv. Energy Mater. **2011**, *1*, 415.

(19) Nakao, Y.; Soneb, K.; Chem. Commum. **1996**, 897.

(20) Kim, J. H.; Kang, M.-S.; Kim, Y. J.; Won, J.; Park, N.-G.; Kang, Y. S.; Chem. Commun. **2004**, 1662.

(21) Akimov, Y. A.; Ostrikov, K.; Li, E. P.; Plasmonics **2009**, *4*, 107.

(22) Akimov, Y. A.; Koh, W. S.; Ostrikov, K.; Optics Express **2009**, *17*, 10195.

Chapter 3. Efficient Light Trapping with Micro-Patterned Three Dimensional Photoanodes in Dye-Sensitized Solar Cells

Reproduced in part of the paper from Sanghyuk Wooh, Hyunsik Yoon, Yong-Gun Lee, Jai Hyun Koh, Yong Soo Kang, and Kookheon Char, Efficient Light Trapping with Micro-Patterned Three Dimensional Photoanodes in Dye-Sensitized Solar Cells (Paper in Revision)

3.1 Introduction

Renewable energy resources have recently gained a great deal of attention due to the ever increasing energy demand, the shortage of fossil fuels, and the growing interest in enviromentally friendly energy scources. Among various kinds of renewable energy sources, solar cells have been regarded as a good candidate because they could capitalize on sunlight as the unlimited energy source. In recent years, the light trapping or harvesting in photovoltaic devices have been extensively explored because of the needs for the reduction of active material thickness to overcome the intrinsic limitations associated with diffusional path length for charge carriers and the charge carrier recombination occurring through interfaces.[1-10] Light absorbance generally decreases with the decrease in the film thickness of a light absorbing active layer, resulting in low energy conversion efficiency. To compensate for lack of light absorption due to

the reduction in the film thickness of the active layer, there have been many trials on how to trap or harvest light efficiently.[4-10] In other words, the light trapping strategy could be quite useful to enhance the power conversion efficiency in the limited film thickness of thin film photovoltaic devices such as dye sensitized solar cells (DSCs)[11-14] and organic photovoltaics (OPVs)[15]. Although many researchers have reported the methods to trap light within thin film solar cells ranging from plasmonics with metallic nanostructures[4, 16] to placing additional scattering layers on top of active thin layers[13], we are still eager to optimize the light absorbance within the active layer for the maximal efficiency of devices.

Here, we demonstrate a light trapping strategy in DSCs with three dimensional photoanodes made from 20 nm TiO_2 nanoparticles, employed for common photo-sensitizing layers. In order to fabricate three-dimensional TiO_2 photoanodes, we exploited the soft lithographic technique, so called a soft molding, with poly(dimethyl siloxane) (PDMS) molds[16]. In the present study, three-dimensional TiO_2 photoanodes with different geometries are realized by adopting the soft molding technique, and their optical and photovoltaic properties are investigated in detail. Over 20 % enhancement in light absorption as well as in the photocurrent of DSCs has been achieved by varying the architecture of TiO_2 photoanodes from two-dimensional flat surface to three-dimensional pyramids. Furthermore, we propose a simple and economical approach to prepare the patterned photoanode with optimized masters for the soft replica molding and also how to integrate the patterned photoanode with a scatterning layer, resulting in the increase in the power conversion efficiency up to 36 % over that based on

the two dimensional planar photoanode.

3.2 Experimental Section

3.2.1 Preparation of PDMS molds for three dimensional structures

The pillar-shaped master was produced by conventional photolithography and the dry etching process. The prism and pyramid masters used in the present study were prepared mechanically. The detailed procedure could be found elsewhere.[20] After the preparation of the masters, we fabricated the PDMS mold by casting PDMS prepolymer on the master. PDMS precursor was used with a mixing ratio of 10:1 (precursor: curing agent) and was cured at 60 °C for 10 hr. To fabricate the inversed pyramid structure, we used a technique of twice replication with polyurethane acrylate (PUA, 301RM, Minuta Tech). After the preparation of the master, drops of PUA prepolymer mixed with an initiator were dispensed onto the master and a flexible PET film as a supporting plane was placed on top of the liquid prepolymer and was lightly pressed. The prepolymers were then exposed to ultra-violet (UV) light (λ = 250 ~ 400 nm) for several seconds (dose = 100 mJ cm^{-2}) through the backside of the transparent PET film for solidification by crosslinking between acrylate functional groups. Then, the cured PUA replica mold on the PET film was removed from the master. For the twice replication, we fabricated PDMS molds by casting on the replicated PUA molds.

3.2.2 Device Fabrication

Electron blocking layer on the FTO glass was formed by spin-coating 0.1

M of Ti (IV) bis(ethyl acetoacetato)-diisopropoxide dissolved in 1-butanol, then sintering at 500 ºC. Flat, two dimensional reference TiO_2 electrodes were fabricated by the doctor blade method with TiO_2 paste ((DSL 18NR-T, Dyesol) onto the FTO substrate (sheet resistance 8 Ω sq^{-1}, Pilkington). In addition, the paste of 150-250 nm anatase TiO_2 particles (WER2-O, Dyesol) was used as a scattering layer. Above the doctor blade coated TiO_2 paste of 7 μm, patterned structures were fabricated by the soft-molding method with the prepared PDMS mold. After pressing the TiO_2 paste at room temperature, samples were annealed at 70 °C for 10 min to remove solvents. The PDMS molds were detached from the patterned TiO_2 microstructures after the first annealing. Then, the solidified TiO_2 electrodes on FTO substrates were sintered at 500 °C for 15 min to entirely remove the organic components of the paste. To adsorb the dye sensitizer, sintered TiO_2 electrodes were dipped in a 0.3 mM N719 dye (cis-bis(isothiocyanato)bis(2,2'-bipyridyl-4,4'-dicarboxylato)-ruthenium (II) bis-tetrabutyl ammonium, Dyesol) in the acetonitrile and tert-butanol solution (1:1 v/v) at 30 °C for 18 hr.

Pt counter electrodes were prepared by thermal decomposition of 0.01 M H_2PtCl_6 in isopropyl alcohol solution spun cast on the FTO substrate at 500 °C for 15 min, and then two holes were made by drill for electrolyte injection. The TiO_2 photoanodes were attached with the counter electrodes using surlyn films (25 μm, Solaronix) which had a role of a spacer between both electrodes. The electrolyte was a mixing solution of 0.6 M 1-methyl-3-propylimidazolium iodide, 0.05 M I_2, 0.05 M guanidinium thiocyanate, and 0.5 M 4-tert-butylpyridine in

acetonitrile. This mixed electrolyte was filled into the holes of the Pt counter electrodes of sandwich structured cells by capillary force, and the holes were subsequently sealed by sulyn films and cover glasses.

3.2.3 Optical Simulation

The light intensity distribution of the three dimensional electrodes were simulated with a commercial optical simulation tool, EM-Explore. The refractive indices of the TiO_2 nanostructures with dyes (including electrolyte in the pore of TiO_2 nanostructure) and the electrolyte were fixed at 2.0 and 1.8, respectively.

3.2.4 Solar cell characterization

The morphologies of patterned TiO_2 electrodes were characterized by field-emission scanning electron microscopy (FE-SEM) using a JSM-5701F (JEOL) instrument. The optical properties of electrodes such as transmission and reflection were characterized by UV/Vis spectroscopy with the integrating sphere (V-670 UV/Vis spectrophotometer, Jasco). The current–voltage characterization of the DSCs was carried by a Keithley 2400 digital source meter and solar simulator with 300W Xenon arc-lamp (Newport) under 1 sun illumination (AM 1.5, 100 mW cm^{-2}). On the front side of a FTO substrate, a light shading mask was applied to except an active area of 0.25 cm^2. The external quantum efficiency of DSCs was analyzed by incident photon to current efficiency measurement (PV measurements, Inc.) as a function of wavelength. The electron lifetime and electron diffusion coefficient in TiO_2 electrodes were evaluated by

intensity-modulated photovoltage spectroscopy under open-circuit conditions and intensity-modulated photocurrent spectroscopy under short-circuit conditions as a function of light intensity through a Controlled Intensity Modulated Photo Spectroscopy system (Zahner) and white light source (Zahner). The detailed measurement conditions are described elsewhere.

3.3 Results and Discussion

3.3.1 Fabrication of Three Dimensional Photoanodes

Figure 3.1 shows the schematic illustration to fabricate three dimensional TiO_2 electrodes by the soft molding method. The soft molding method[17], which is classified as one type of soft lithographies, employs a PDMS mold to absorb the evaporated solvent of a TiO_2 paste while filling the TiO_2 paste into the void space of the mold. After preparing the masters by conventional photolithography or micromachining technique, we prepared the replica molds from the masters with either polyurethane acrylate (PUA, 301RM, Minuta Tech)[18] or PDMS. We used the PDMS precursor with a mixing ratio of 10:1 (precursor:curing agent) and cured it at 60 °C for 10 hr. The cured PDMS molds were manually removed and cut prior to use. In order to prepare inverted pyramid structures of TiO_2, PUA molds were first replicated from the original master, followed by the sequential replication of the PUA replica with PDMS.

We prepared patterned photoanodes of DSCs by first layering electron blocking layers on FTO substrates and then coating with a higly viscous TiO_2 paste by the doctor blade method to yield a film thickness of ~7 μm. After gentle pressing the TiO_2 paste film at room temperature with PDMS molds prepared to guarantee full conformal contacts, we annealed the TiO_2 paste film/PDMS mold pair for 10 min at 70 °C to remove residual solvent. The molds were then detached from the patterned TiO_2 films and the partially solidified TiO_2 structures

attached to FTO substrates were further sintered at 500 °C for 15 min. The sintered TiO_2 electrodes were then dipped into the N719 dyes dissolved in acetonitrile and tert-butanol mixed solvent to let the dye sensitizers be adsorbed on the surfaces of TiO_2 photoanodes. Figures 3.1 b-e show the scanning electron microscopy (SEM) images of the patterned TiO_2 photoanodes with pillars (Figure 3.1 b), prisms (Figure 3.1 c), pyramids (Figure 3.1 d), and inverted pyramids (Figure 3.1 e). It is noted that the feature sizes are in the micron-range which is much greater than the wavelength of visible or infrared light. As shown in Figures 3. 1b-e, those patterned electrodes were, indeed, well defined and uniform with TiO_2 nanoparticles over the large surface area (Figure 3.2).

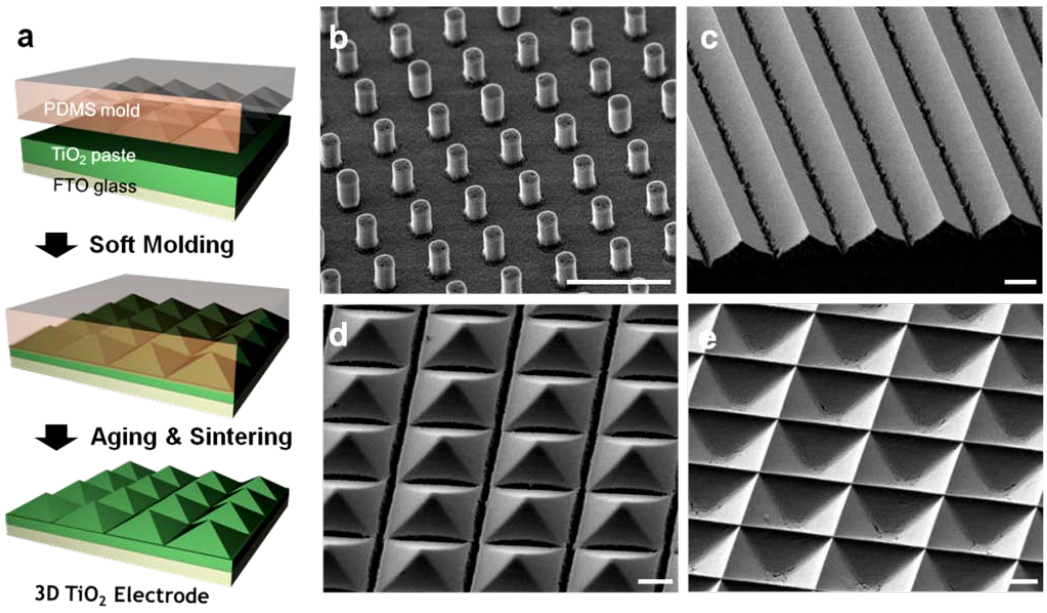

Figure 3.1. a, a schematic illustration for the fabrication of a three dimensional TiO_2 photoanode. SEM images of **b,** pillar; **c,** prism; **d,** pyramid; **e,** inverted pyramid-patterned TiO_2 photoanodes consisting of 20 nm TiO_2 nanocrystals (scale bars in SEM pictures: 10 μm).

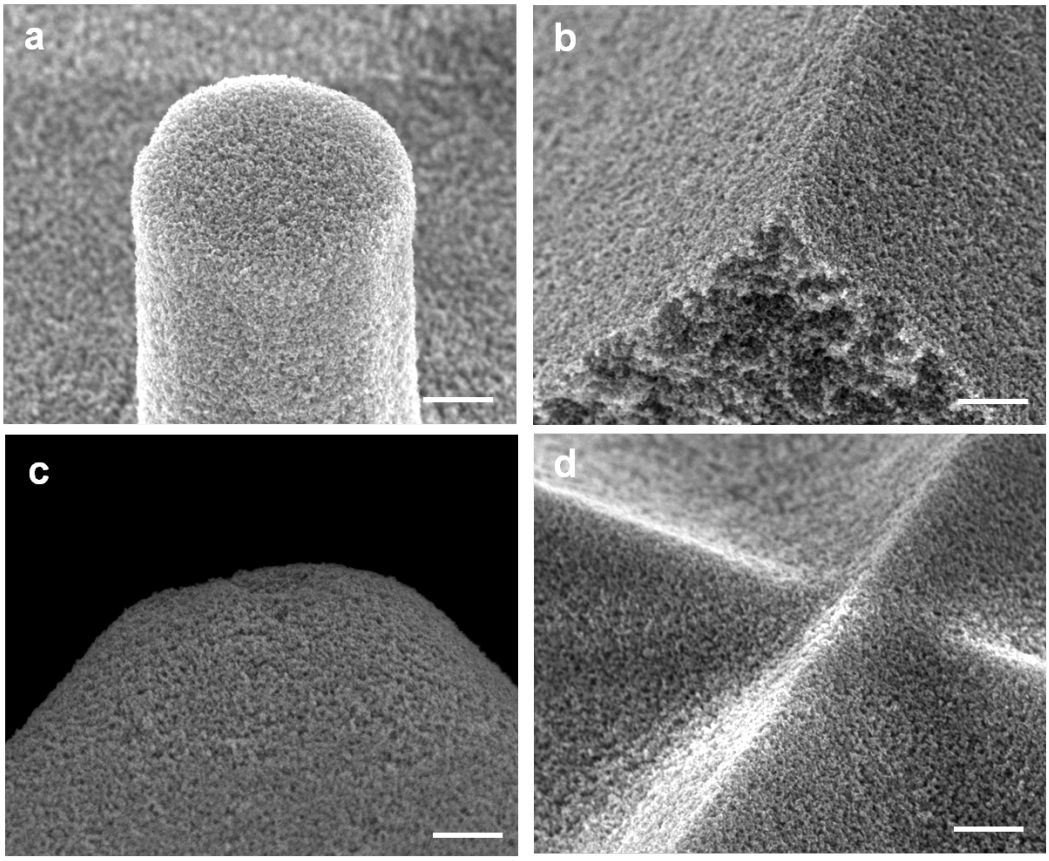

Figure 3.2. Magnified scanning electron microscope (SEM) images of patterned TiO_2 photoanodes with a shape of (a) a pillar, (b) a prism, (c) a pyramid, and (d) an inverted pyramid. (Scale bar: 500 nm)

3.3.2 Optical and Photocurrent-Voltage Characteristics of DSCs with Three Dimensional Photoanodes

After the soft molding, we compared the absorption properties and photovoltaic performance of the patterned photoanodes with different geometries. The two dimensional and three dimensional photoanodes have the same amount of TiO_2 nanoparticles and dye loading, which is confirmed by the dye loading test after detaching the dyes from the TiO_2 films (Figure 3.3). Although the patterned photoanodes adsorb the same amount of dyes, the three dimensional photoanodes were found to trap more light than the conventional two dimensional flat photoanode, as shown in darker red color in Figure 3.4 a. Among the three dimensional photoanodes tested, the pyramid-patterned photoanode traps even more light than the prism-patterned photoanode. The UV/Vis absorption spectra, calculated by the measured transmission (T) and reflection (R) (Absorption (%) = 100 – T – R), were obtained with an integrating sphere[18], as shown in Figure 3.4 b and Figure 3.5. As we anticipated with visual examination of the photoanodes shown in Figure 3.4 a, the three dimensional photoanodes show the significant increae in absorbance related to the enhanced light trapping capability of the patterned photoanodes. In addition, the pyramid-patterned TiO_2 photoanode has the highest light absorption, compared to other patterned photoanodes. We note that the pyramid-patterned photoanode has the most effective light trapping capability due to the total internal reflection by the four triangular sloping sides, which is in good agreement with the quantitative

analysis of Smith et al.[3] Smith et al. compared the light trapping characteristics for different geometries such as slabs, upright pyramids, and inverted pyramids, demonstrating that the inverted pyramid structures show the highest path length enhancement. In the case of DSCs, since the incident light is illuminated on a transparent FTO substrate, the effect of inverted pyramids in silicon solar cells is the same as the effect with the upright pyramid-patterned photoanodes.

The light intensity distribution of the pyramid-shaped photoanode was calculated by a commercial optical simulation tool, as shown in Figure 3.4 c. We fixed the refractive indices of TiO_2 nanostructure containing dyes (including electrolytes within the pores of the TiO_2 nanostructure) and the electrolyte at 2.0 and 1.33, respectively[19]. The simulation result shows that the light intensity of the pyramid-shaped photoanode is higher than that of the two dimensional flat TiO_2 photoanode (Figure 3.6) This is because the incident light is focused by the total internal reflection at the interfaces of TiO_2 tilted facets in contact with bulk electrolyte. Figure 3.4 d shows the photocurrent-voltage (J-V) characteristics of DSCs with photoanodes with different surface patterns. The pyramid-patterned TiO_2 photoanode represents the highest photocurrent (J_{SC}) as well as the power conversion efficiency (PCE) due to the increase in the amount of trapped light, as anticipated from the absorption properties.

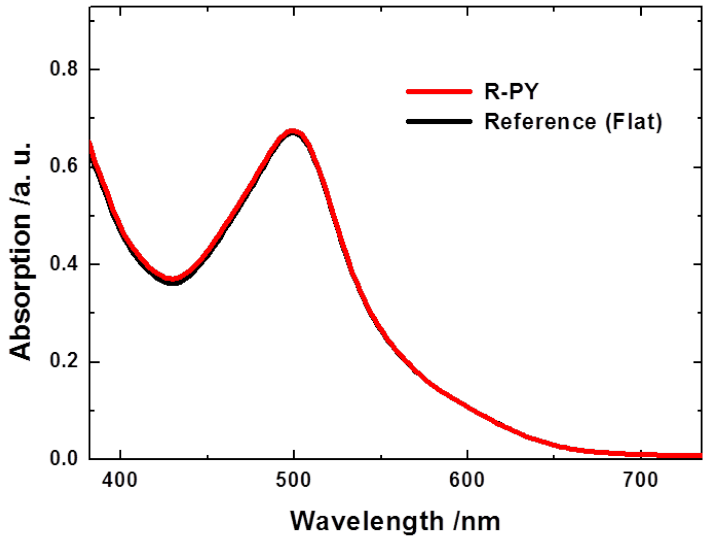

Figure 3.3. UV/Vis spectroscopic graphs representing amounts of dyes adsorbed in a two dimensional (black) and a three dimensional randomized pyramid-patterned (R-PY) (red) TiO_2 photoanode. We characterized the amounts after detaching dyes from TiO_2 surface with 10 mM NaOH solution.

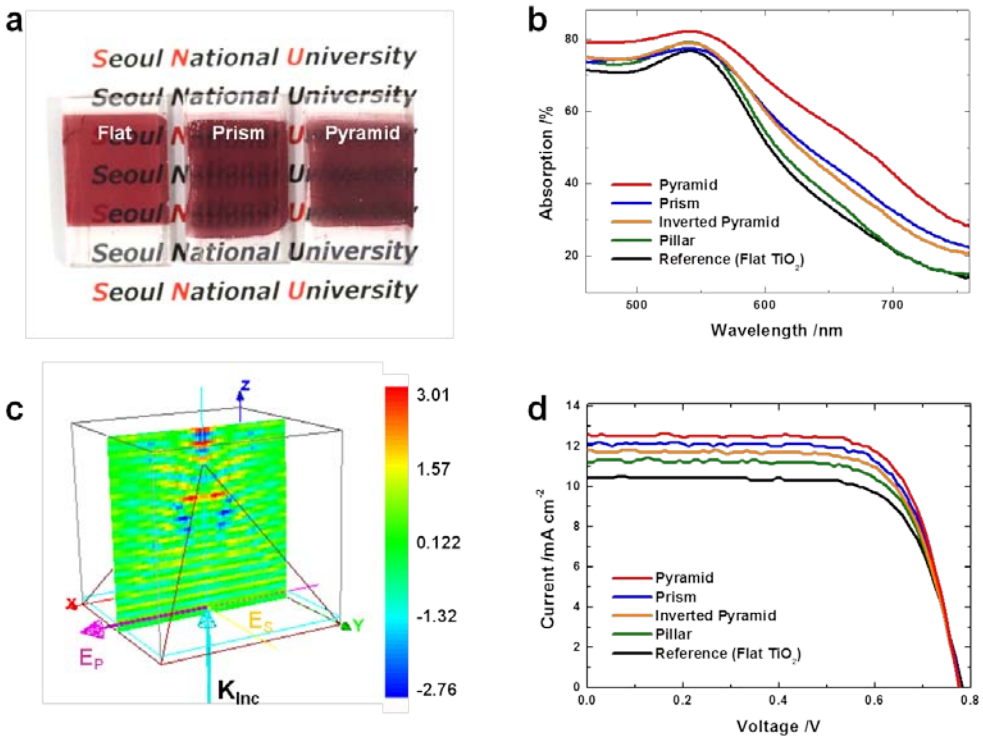

Figure 3.4. **a,** a photo of two dimensional (flat), prism-patterned, and pyramid-patterned TiO_2 photoanodes containing N719 dyes. **b,** light absorption characteristics of two- and three-dimensional TiO_2 photoanodes with different geometries after N719 dye loading, characterized by UV/Vis spectroscopy with an integrating sphere. **c,** the light intensity distribution in a pyramid–patterned photoanode calculated by an optical simulation tool. **d,** the photocurrent-voltage characteristics of DSCs with photoanodes with different geometries, measured under 1 Sun illumination (AM 1.5 and 100 mW cm^{-2}) with shading masks (active area: 0.25 cm^2).

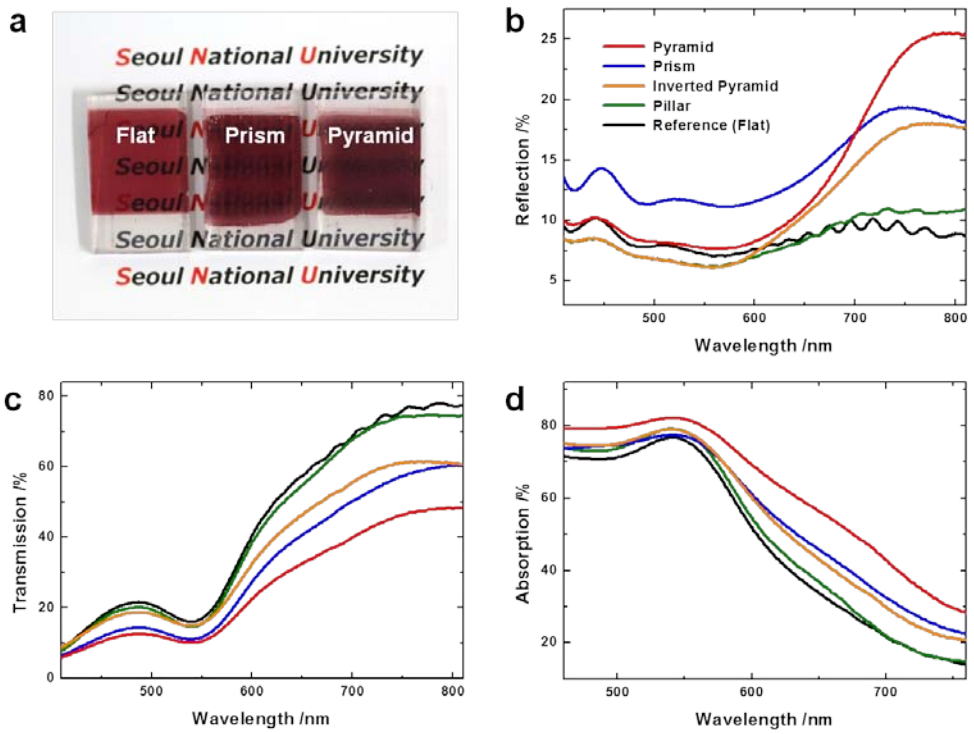

Figure 3.5. Optical properties of two dimensional and three dimensional TiO_2 photoanodes of different geometries after N719 dye adsorption, characterized by (a) photo and UV/Vis spectroscopy with an integrating sphere, ((b) reflection, (c) transmission, and (d) absorption).

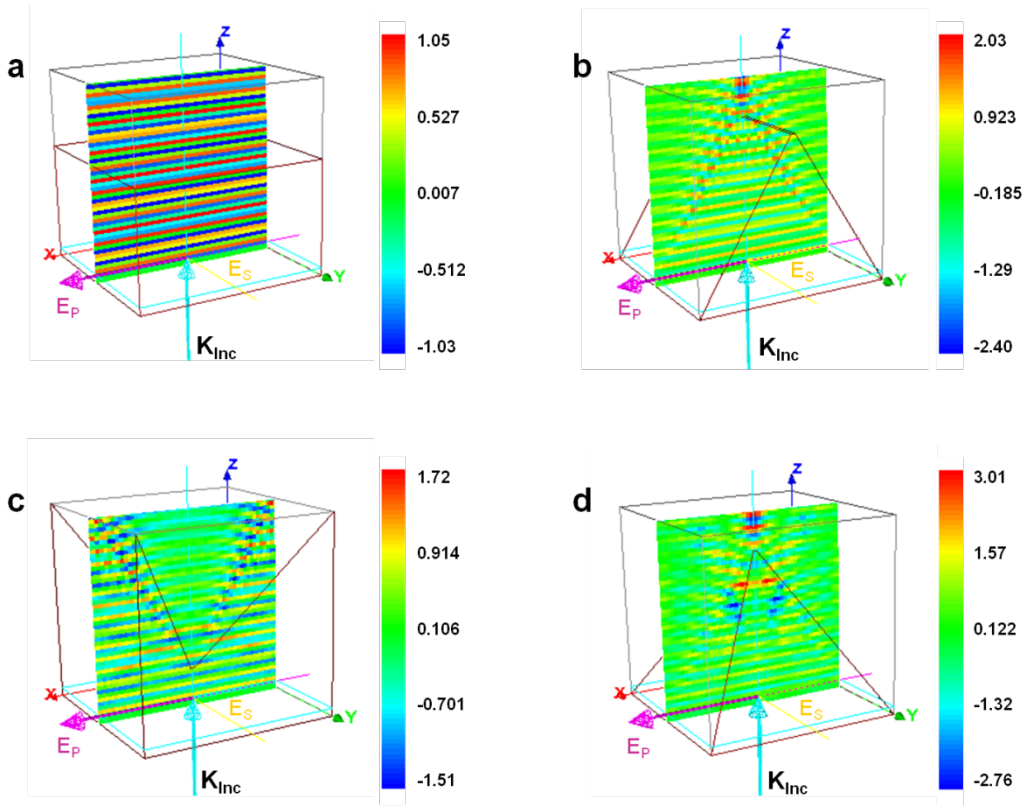

Figure 3.6. Comparison of intensity distributions of 550 nm wavelength light in (a) flat, (b) prism, (c) inverted a pyramid, and (d) pyramid–patterned TiO_2 photoanodes, calculated by an optical simulation tool. Refractive indices of TiO_2 nanostructure (including dyes and electrolytes within the mesoporous TiO_2) and the electrolyte are given by 2.0 and 1.33, respectively.

3.3.3 Three Dimensional Randomized Pyramid Photoanodes

Although the soft molding method is proven to be quite effective in realizing three dimensional structures at low cost over large area, there still exists a difficulty in preparing three dimensional pattern masters by complicated semiconductor processing or mechanical machining, which is time consuming and expensive. Inspired by the texturing of silicon wafers by wet etching, we prepared a textured silicon wafer[2] and employed this as a master for PDMS replication. With the PDMS replica molding, we were able to realize the randomized pyramid-shaped TiO_2 photoanode in a much simpler and the cheapest possible way. The texturing of crystalline silicon substrates with anisotropic wet etching to yield surfaces covered by randomly distributed pyramids with different size defined by intersecting (111) crystallographic planes is a well known technique.[2] A silicon (100) wafer was etched in an etchant (KOH/isopropyl alcohol (IPA) 10/10 wt% in deionized water) at 70 °C for 40 min. Figure 3.7 b shows the SEM image of the anisotropically etched silicon wafer surface. The pyramidal structures thus could be easily obtained, with size ranging from 1 to 10 μm. We used the anisotripically etched silicon substate as an original master and replicated it with PDMS to realize a randomized pyramid-shaped TiO_2 photoanode (denoted as R-PY) by the soft molding over large area. As shown in the SEM image of Figure 3.7 c, d , the TiO_2 photoanode successfully transferred the shape-shape of the original silicon master shown in Figure 3.7 b. This method produces easy and cheap process for fabricating three

dimensional pyramid photoanodes with efficient light trapping structures.

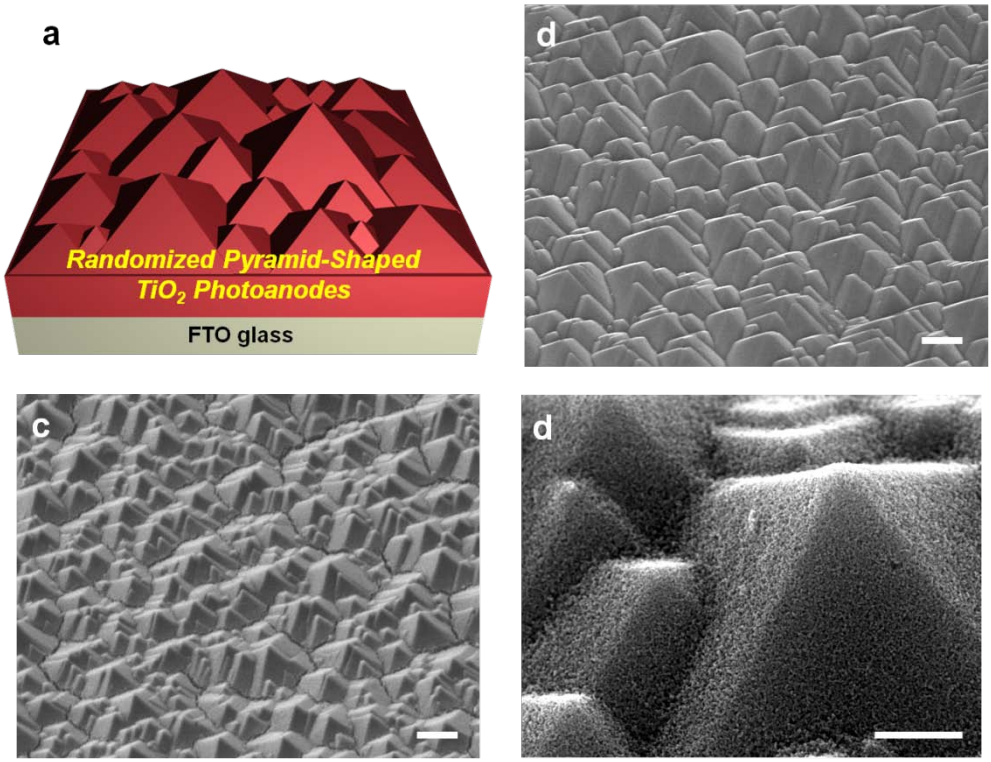

Figure 3.7. **a,** a schematic illustration for the randomized pyramid-shaped TiO_2 photoanode. A SEM image of **b,** randomized pyramid silicon surface, used as a pattern master, created by the anisotropic wet etching process and **c,** randomized pyramid TiO_2 photoanode prepared by the replica mold of the silicon master **b. d,** high magnification image of **c**. (scale bars in the pictures: 1 μm (b, c), 5 μm (d)).

3.3.4 Three Dimensional Randomized Pyramid Photoanodes with Additional Scattering Layer

To maximize the light trapping in DSCs, we combined a scattering layer with three dimensional TiO_2 photoanodes, more specifically with the R-PY photoanode. Figure 3.8 b shows the cross-sectional SEM image of a scattering layer consisting of TiO_2 particles in size of 150 – 250 nm, coated on the R-PY photoanode. The photocurrent-voltage (J-V) characteristcs of different types of photoanodes including the composite photoanode were obtained under 1 Sun condition (AM 1.5, 100 mW cm^{-2}) with shading masks, as shown in Figure 3.8 c. We note that the R-PY photoanode alone shows slightly higher J_{SC} and PCE values when compared with the values obtained from the regularly arranged pyramid photoanode, as summarized in Table 3.1. We believe that this is mainly due to the fact that the R-PY photoanode removes the geometrical sensitivity of the regular-shaped photoanode. In particular, by the combination of randomized pyramids with a scattering layer, a remarkable increase in PCE is achieved owing to the significant increase in Jsc over 36 % of the conventional two dimensional flat TiO_2 photoanode. It is remarkable to note that the addition of the scattering layer could be still contributed to the increase in the performance of the three dimensional photoanodes. This enhancement in the J-V characteristics is also found to agree well with the results of incident photon-to-current efficiency (IPCE) measurement and UV/Vis spectra obtained with an integrating sphere, verifying that the enhancement of J-V characteristics is attributed to the

extremely efficient light trapping originating from the combination of both effects. (Figure 3.9) Further investigation with intensity-modulate photovoltage spectroscopy (IMVS) and intensity-modulate photocurrent spectroscopy (IMPS) indicates that the electron lifetimes and diffusion coefficients are nearly the same in both two dimensional flat and randomized pyramid-shaped TiO_2 photoanodes, corresponding to the constant open-circuit voltages (V_{OC}) and fill factors (FF), as shown in Table 3.1. There is a strong evidence that three dimensional photoanode structures make light trapping more efficient without giving any deleterious side effects such as the increase in electron recombination (Figure 3.10).

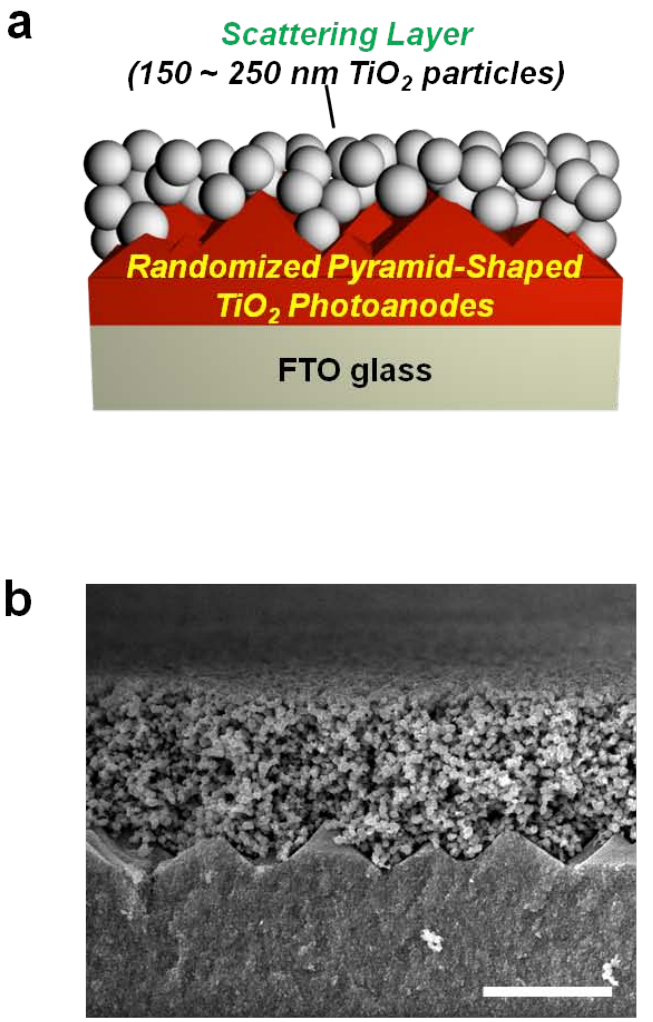
a
Scattering Layer
(150 ~ 250 nm TiO2 particles)
Randomized Pyramid-Shaped
TiO2 Photoanodes
FTO glass
b
c
Current /mA cm-2
Voltage /V
0
4
8
12
0.0
0.2
0.4
0.6
0.8
Scatteing Layer on R-PY
Scatteing Layer on Flat TiO2
R-PY
Reference (Flat TiO2)

Figure 3.8. **a,** a schematic illustration and **b,** a SEM image of scattering layer coated randomized pyramid-shaped TiO_2 photoanode. **c,** the photocurrent-voltage characteristics of DSCs with photoanodes of scattering layer coated randomized pyramid-shaped TiO_2 photoanode, measured under 1 Sun illumination (AM 1.5 and 100 mW cm^{-2}) with shading masks (active area: 0.25 cm^2).

Table 3.1. Photovoltaic characteristics of DSCs with photoanodes of different geometries[a]

	V_{OC} (V)	J_{SC} (mA cm^{-2})	FF	Efficiency (%)
Flat TiO_2	0.78	10.3	0.73	5.89
Pillar TiO_2	0.78	11.1	0.72	6.13
Prism TiO_2	0.78	12.1	0.72	6.77
Inverted Pyramid TiO_2	0.78	11.7	0.72	6.59
Pyramid TiO_2	0.78	12.4	0.73	6.94
R-PY[b]	0.77	12.5	0.72	6.99
Flat TiO_2 with a Scattering Layer	0.78	13.3	0.73	7.5
R-PY with a Scattering Layer	0.78	14.5	0.72	8.02

[a] Sensitizer: N719 dye; electrolyte: LiI (0.1M), MPII (0.6M), I_2 (0.05M), tBP (0.5M), and GuSCN (0.05M) dissolved in acetonitrile; measured under 1 Sun illumination (AM 1.5 and 100 mW cm^{-2}) with shading masks (active area: 0.25 cm^2).

[b] R-PY: randomized pyramid-patterned TiO_2 photoanode.

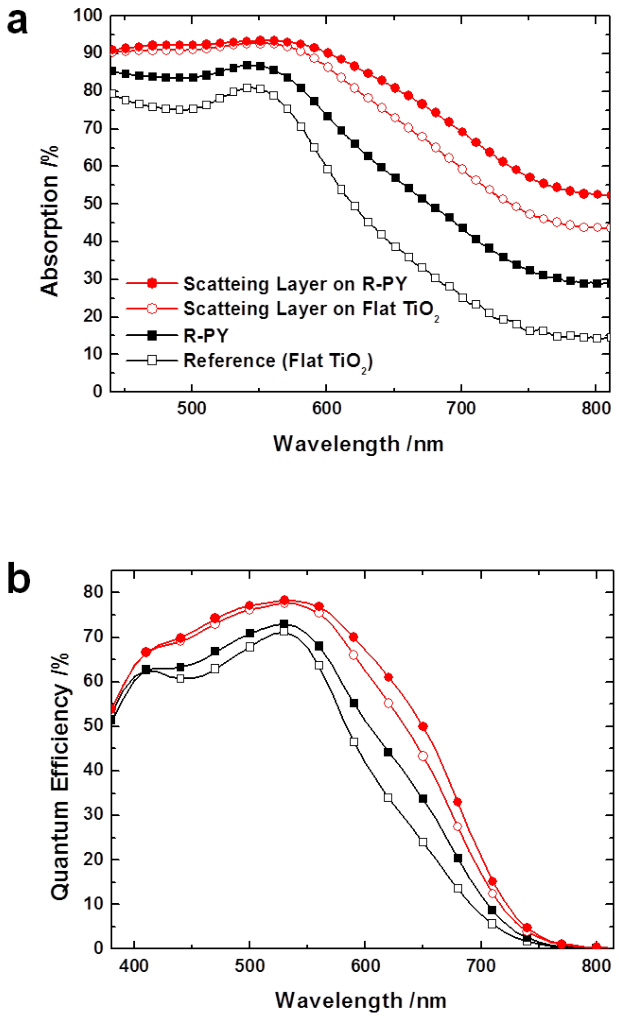

Figure 3.9. (a) Absorption spectrums characterized by UV/Vis spectroscopy with an integrating sphere and (b) Incident photon-to-current efficiency (IPCE) of two dimensional and randomized pyramid-patterned TiO_2 photoanodes, employing additional scattering layers.

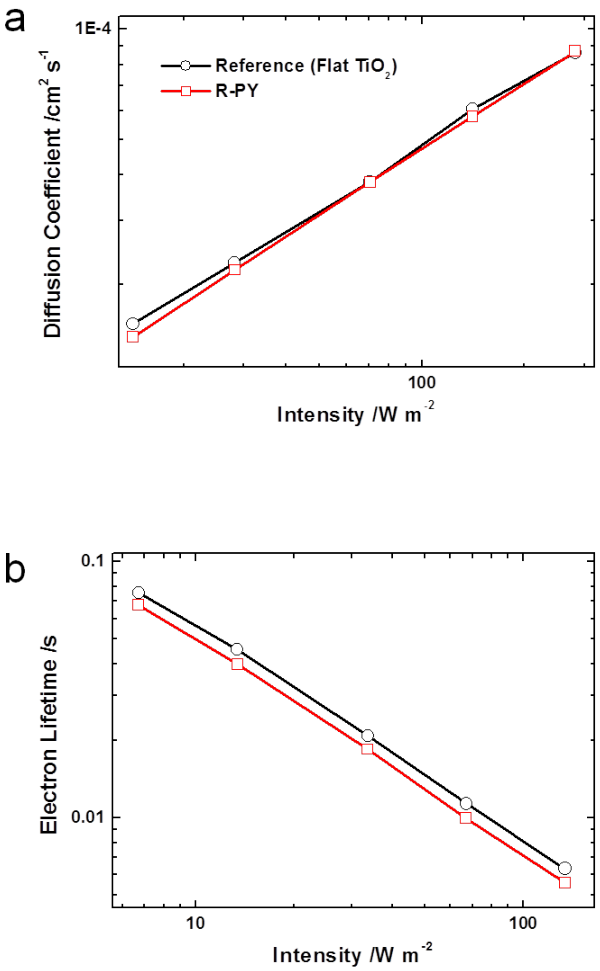

Figure 3.10. (a) Electron diffusion coefficient and (b) lifetime of two dimensional and randomized pyramid-patterned TiO_2 photoanodes in DSCs, characterized by an intensity-modulate photocurrent spectroscopy (IMPS) and an intensity-modulate photovoltage spectroscopy (IMVS), respectively.

3.4 Conclusion

In conclusion, we present a highly efficient and simple light trapping strategy in fabricating novel three dimensional photoanode to improve the energy conversion efficiency of DSCs. The three dimensional TiO_2 photoanode structures were prepared by the soft molding method with PDMS molds. Among the different photoanode geometries tested, the pyramid-shaped TiO_2 photoanode shows the hightest light absorbance and consequently the best photocurrent-voltage performance, due to the total light reflection off the interfaces between the TiO_2 photoanode and bulk electrolyte. Another simple approach was proposed to prepare random pyramid photoanodes at low cost based on the wet etching of silicon wafers. The combination of the three-dimensional random pyramid photoanode with a scattering layer further increased the power conversion efficiency up to 36 % compared with the value obtained from the two-dimensional flat photoanode.

3.5 References

(1) Yablonovitch, E. J. Opt. Soc. Am. **1982**, *72*, 899.

(2) Campbell, P.; Green, M. A. J. Appl. Phys. **1987**, *62*, 243.

(3) Smith, A. W.; Rohatgi, A. Sol. Energy Mater. Sol. Cells **1993**, *29*, 37-49.

(4) Atwater, H. A.; Polman, A., Nat. Mater. **2010**, *9*, 205.

(5) Battaglia, C.; Escarré, J.; Söderström, K.; Charriére, M.; Despeisse, M.; Haug, F.; Ballif, C. Nat. Photonics **2011**, *5*, 535.

(6) Kim, J. B.; Kim, P.; Pegard, N. C.; Oh, S. J.; Kagan, C. R.; Fleischer, J. W.; Stone, H. A.; Loo, Y. –L. Nat. Photonics **2012**, *6*, 327.

(7) Zhu, J.; Hsu, C.; Yu, Z.; Fan, S.; Cui, Y. Nano Lett. **2010**, *10*, 1979-1984.

(8) Battaglia, C. et al. Nano Lett. **2010**, *11*, 661.

(9) Catchpole, K. R.; Mokkapati, S.; Beck, F.; Wang, E.; McKionley, A.; Basch A.; Lee, J. MRS Bull. **2011**, *36*, 461.

(10) Mallick, S. B.; Sergeant, N. P.; Agrawal, M.; Lee, J.; Peumans, P. MRS Bull. **2011**, *36*, 453.

(11) Grätzel, M. Nature **2009**, *414*, 338.

(12) Grätzel, M. Acc. Chem. Res. **2009**, *42*, 1788.

(13) Ito, S.; Zakeeruddin, S. M.; Humphry-Baker, R.; Liska, P.; Charvet, R.; Comte, P.; Nazeeruddin, M. K.; Péchy, P.; Takata, M.; Miura, H.; Uchida, S.; Grätzel, M. Adv. Mater. **2006**, *18*, 1202.

(14) Hore, S.; Vetter, C.; Kern, R.; Smit, H.; Hinsch, A. Sol. Energy Mater. Sol. Cells **2006**, *90*, 1176.

(15) Lee, J. H.; Kim; D. W.; Jang, H.; Choi, J. K.; Geng, J.; Jung, J. W.; Yoon, S. C.; Jung, H.-T. Small. **2009**, *5*, 2139.

(16) Ding, I.; Zhu, J.; Cai; W., Moon, S.; Cai, N.; Wang, P.; Zakeeruddin, S. M.; Grätzel, M.; Brongersma, M. L.; Cui, Y.; McGehee, M. D. Adv. Energy Mater. **2011**, *1*, 52.

(17) Kim, Y. S.; Suh, K. Y.; Lee, H. H. Appl. Phys. Lett. **2001**, *79*, 2285.

(18) Brown, M. D.; Suteewong, T.; Kumar, R. S. S.; D'Innocenzo; V., Petrozza, A.; Lee; M. M.; Wiesner, U.; Snaith, H. J. Nano Lett. **2011**, *11*, 438.

(19) Mihi, A.; López-Alcaraz, F. J.; Miguez, H. Appl. Phys. Lett. **2006**, 88, 193110.

(20) Yoon, H.; Oh, S. G.; Kang, D. S.; Park, J. M.; Choi, S. J.; Suh, K. Y.; Char, K. & Lee, H. H. Nat. Comm., **2011**, 2:455.

국문 초록

빛 에너지를 전기 에너지로 전환시켜주는 광 변환 기술은, 태양으로부터 반 영구적으로 유입되는 빛 에너지를 다양한 쓰임으로 활용할 수 있게 한다는 장점 때문에 신 재생에너지 개발 분야에서 많은 연구가 진행 중에 있다. 광 변환 기술을 이용해 개발된 태양전지는 빛 에너지를 받아 전기 에너지로 내보내는 발전 소자로써, 소자의 광 변환 효율은 흡수한 빛의 양과 비례한다. 때문에 빛을 더 효과적으로 수집하여 이용하기 위한 광 수집 기술 및 변환 기술은 태양전지의 성능 향상을 위해 반드시 필요한 핵심 기술들이라 할 수 있다. 본 연구에서는 높은 효율과 낮은 공정 단가 때문에 차세대 태양전지로 각광받는 염료감응 태양전지의 광 수집 효율을 높이기 위한 연구를 크게 세 가지 단계로 개발하여 진행하였으며, 각 장의 주요 내용은 다음과 같다.

제 1 장에서는 염료가 흡수한 빛 에너지를 효과적으로 전기 에너지로 변환시키기 위해 TiO_2 나노 반도체 산화물 표면에 먼저 염료를 흡착 시킨 후 초소수성 공흡착제로 자기 조립 단층을 추가적으로 형성시켜, 염료에서 주입된 주입전자가 다시 전해질 층으로 돌아가 손실되는 재결합 반응을 최소화하는 연구를 정리 하였다. 염료의 바닥상태에 있던 전자는 빛 에너지를 흡수하여 들뜬 상태로 전이 한 후 나노 반도체 산화물로 주입이 된다. 하지만 많은 양의 주입전자가 전극까지 도

달하지 못하고 전해질의 산화-환원 이온 종과 반응하여 손실이 되는데, 이러한 반응은 염료가 흡착되어 있지 않은 전해질과 직접 맞닿은 나노 반도체 산화물 표면에서 일어나게 된다. 따라서 염료를 붙인 나노 반도체 산화물 표면에 초소수성 특징을 갖는 공흡착제로 자기 조립 단층을 추가적으로 형성하여 전해질로부터의 절연을 유도 하였으며, 재결합 반응의 감소를 전기화학 분석을 통해 확인하였다. 또한 기존에 연구되어온 공흡착제는 첨가 시 흡착되는 염료의 손실이 있었던 것에 반해, 순차 담지 기법을 통해 염료의 손실 없이 소자의 개방전압 및 광 변환 효율을 효과적으로 향상시키는 결과를 얻었고, 기존의 널리 이용되는 공흡착제에 순차적 흡착 방법을 이용하여 추가적인 효율 증가를 갖는 전극을 구현하였다.

제 2 장에서는 금 나노입자의 표면 플라즈몬 공명 현상을 이용해 광전극 내에서 염료가 흡수하는 빛 에너지를 증가시키는 연구에 대한 결과를 정리하였다. 먼저 수용액 상에서 합성한 금 나노입자를 염료감응 태양전지 광전극에 균일하게 분포시키고 전해질 및 나노 반도체 산화물과의 직접 접촉을 피하기 위해 약 10 nm 두께의 실리카 껍질을 표면에 형성시켰다. 이렇게 만들어진 금 @ 실리카 나노입자를 TiO_2 나노 반도체 산화물 페이스에 섞어 투명 전도성 유리 위에 코팅하는 방법으로 광전극을 형성하였고, 금 나노입자의 표면 플라즈몬 공명에 의한 광전극 내에서의 빛 에너지 흡수 증가를 관찰할 수 있었다. 이에

더해 광전극에서의 빛 에너지 흡수 증가가 표면 플라즈몬 공명에 의한 효과임을 증명하기 위해, 금 @ 실리카 나노입자를 함유한 광전극과 구조는 일치하지만 표면 플라즈몬 공명 현상은 발생하지 않는 속이 빈 실리카 입자를 함유한 광전극을 구현하는 금 나노입자 부식 방법 개발하였다.

제 3 장에서는 소프트 임프린팅 기술을 이용해 나노 반도체 산화물을 3차원 마이크로 구조로 구현한 연구 결과를 정리하였다. 지금까지의 염료감응 태양전지 광전극은 모두 평평한 2차원 구조로, 빛 에너지 흡수를 증가시키는 방법으로 오직 추가적인 산란층을 형성시키는 방법만이 사용되어왔다. 하지만 임프린팅 기술을 이용해 3차원 마이크로 구조로 광전극을 구현한 결과 전해질과의 계면에서 발생하는 전반사 및 구조에 따른 광 투과 길이가 길어지는 효과로 빛 에너지의 흡수가 효과적으로 증가함을 관찰하였다. 여러 가지 구조들 중 피라미드 구조에서 가장 높은 흡수율이 나타났으며, 이러한 흡수 증가를 시뮬레이션을 통해 증명하였다. 이러한 3차원 구조는 마스터의 제조 공정 단가가 비싸다는 단점이 있는데, 기존에 널리 알려진 실리콘 습식식각 방법을 이용해 저렴하고 간단한 피라미드 마스터 제조 공정을 개발하였다. 더욱이 3차원 구조 위에 산란층을 추가적으로 형성 시켰을 때 산란층에 의한 효과와 3차원 구조에 의한 광 투과 길이의 증가 효과가 중첩되어, 빛 에너지 흡수와 소자의 광변환 효율이 극대화 되는 결과

를 얻을 수 있었다.

주요어: 광자 수집 이용, 염료감응 태양전지, 초소수성 공흡착제, 표면 플라즈몬 공명, 삼차원 광전극

학 번: 2008-30262